Raúl Erades de Quevedo

Analysis of the effect of saturation gas, solution temperature and concentration on OH radical formation by ultrasonic irradiation for hydrogen production optimization

Master's thesis in TEP4900
Supervisor: Bruno G. Pollet
June 2019

Norwegian University of Science and Technology
Faculty of Engineering
Department of Energy and Process Engineering

NTNU
Norwegian University of
Science and Technology

Abstract

There is an increasing need to improve the way we obtain and use energy, as with traditional methods planet Earth is becoming less and less habitable. In this regard, the use of hydrogen as a clean energy vector has acquired special relevance nowadays. The production of hydrogen is still expensive and mostly not environmentally friendly; however, it is expected to change in the coming years. One of the areas being investigated for a better and cleaner production of hydrogen is the use of power ultrasound. Although this technology still needs further research, it has already shown promising results. The application of ultrasound to an aqueous solution can certainly lead to synthesize hydrogen, as well as improving mass transfer in an electrochemical process such as electrolysis.

In this master's thesis, Weissler and Fricke dosimetry methods are used in order to characterize the formation of hydroxyl radicals by ultrasonic radiation using a simple 24 kHz frequency ultrasound generator. The importance of a greater quantity of OH radicals lies in their impact in hydrogen production, since these particles can interact with others to form this element. The effects of different dissolved gases (argon, nitrogen and air) are analyzed, as well as the effect of the initial temperature of the solution with the purpose to analyze its impact on the formation of OH radicals. The effect of the concentration of KI with the Weissler dosimetry is also analyzed. It is discussed the most suitable combination of these parameters that enhance OH radical obtention and potentially, hydrogen production. An overview is also provided about the main mechanisms of power ultrasound and its relation to sonochemical production of hydrogen, including an outline of the main dosimetry methods.

Acknowledgement

I want to thank Bruno G. Pollet and Md Hujjatul Islam for their useful guidance and their availability to help me with this Master's Thesis. I would also like to thank Paol Geffroy and Antoine Le Bouder for their great contribution and support. I cannot either forget to thank all my lab partners, who taught me a lot of things. Among them I would particularly want to express my gratitude to Lars Martin Ingebrigtsen for his important input and his good counsel.

Finally, I want to thank my parents and friends for providing me unfailing support in the course of this work.

Table of Contents

1 Introduction 1

2 Theoretical Background 2

2.1 Power ultrasound and Sonochemistry 2

2.1.1 Introduction to Sonochemistry 2

2.1.2 Phenomena associated to Power Ultrasound 3

2.1.3 Ultrasound systems 5

2.2 Power ultrasound and hydrogen production 7

2.2.1 Mechanisms of sonochemical production of hydrogen 7

2.2.2 Parameters that affect sonochemical activity 9

2.3 Dosimetry methods 11

2.3.1 Weissler dosimetry 12

2.3.2 Fricke dosimetry 13

2.3.3 Other dosimetry methods 13

3 Materials and Methods 14

3.1 Experimental setup and materials 14

3.2 Experimental procedure 17

3.3 Major setbacks 20

4 Results and Discussion 22

4.1 Weissler dosimetry 22

4.1.1 Nitrogen 22

4.1.2 Argon 24

4.1.3 Air 26

4.1.4 Effect of the water loop overpressure in sonochemical activity 27

4.2 Fricke dosimetry 28

4.3 Additional remarks and limitations of this work 29

5 Conclusion 32

Bibliography 33

Appendix A Experimental plan i

Appendix B Gas saturation time tests iii

Appendix C Results iv

a) Weissler dosimetry with nitrogen iv

b) Weissler dosimetry with argon v

c) Weissler dosimetry with air vi

d) Fricke dosimetry tests vii

List of Figures

Figure 1: Physical effects produced by ultrasonic irradiation in a liquid solution [10] 3
Figure 2: Ultrasonic horn and ultrasonic bath schemes 5
Figure 3: Erosion effects observed in an ultrasonic horn made with titanium 6
Figure 4: Production of hydrogen by acoustic cavitation [7] 8
Figure 5: Besançon microsonoreactor (15 mm) 14
Figure 6: Main elements of the cell 15
Figure 7: Overview of the setup 16
Figure 8: Comparison between the pressurized recirculated solution and the cell 18
Figure 9: Functioning scheme about the experimental setup during sonication 19
Figure 10:Testing of samples with Helios Gamma spectrophotometer 20
Figure 11: Some of the issues experienced during the experiments 21
Figure 12: Effect of potassium iodide concentration on triiodide production for different initial solution temperatures, using nitrogen as a saturated gas and a frequency of 24 kHz. Water loop overpressurized (1,5 bar) 23
Figure 13: Effect of the initial solution temperature on triiodide production for different concentrations of potassium iodide, using nitrogen as a saturated gas and a frequency of 24 kHz. Water loop overpressurized (1,5 bar) 24
Figure 14: Effect of potassium iodide concentration on triiodide production for different initial solution temperatures, using argon as a saturated gas and a frequency of 24 kHz. Water loop overpressurized (1,5 bar) 25
Figure 15: Effect of the initial solution temperature on triiodide production for different concentrations of potassium iodide, using argon as a saturated gas and a frequency of 24 kHz. Water loop overpressurized (1,5 bar) 25
Figure 16: Effect of potassium iodide concentration on triiodide production for different initial solution temperatures, using air as a saturated gas. and a frequency of 24 kHz. Water loop overpressurized (1,5 bar) 26
Figure 17: Effect of the initial solution temperature on triiodide production for different concentrations of potassium iodide, using air as a saturated gas and a frequency of 24 kHz. Water loop overpressurized (1,5 bar) 27
Figure 18: Impact of water loop overpressure in sonochemical activity at a frequency of 24 kHz 28
Figure 19: Effect of the initial solution temperature on ferric ion production for a standard concentration in the Fricke dosimetry ($NH42FeSO42 \bullet 6H2O$ $(0{,}001\ mol/l)$, $H2SO4$ $(0{,}4\ mol/l)$ and $NaCl$ $(0{,}001\ mol/l)$), using air and argon as a saturated gases and a frequency of 24 kHz. Water loop overpressurized (1,5 bar) 29
Figure 20: Effect of the initial solution temperature on triiodide production using air, nitrogen and argon as saturated gases with a concentration of 1M KI and a frequency of 24 kHz. Water loop overpressurized (1,5 bar) 30
Figure 21: Dissolved oxygen evolution for nitrogen during the DO tests iii
Figure 22: Dissolved oxygen evolution for argon during the DO tests iii
Figure 23: Dissolved oxygen evolution for air during the DO tests iii

List of Tables

Table 1: Tolerance and relative errors of the flasks employed 16
Table 2: Mass of chemical compound needed for each test using a 200 ml flask 17
Table 3: Properties of the different gases under consideration for this work [60], [61] 30
Table 4: Programmed tests for nitrogen by means of the Weissler dosimetry method i
Table 5: Programmed tests for argon by means of the Weissler dosimetry method i
Table 6: Programmed tests for air by means of the Weissler dosimetry method ii
Table 7: Programmed tests for the optimum gas in the Weissler dosimetry experiments by means of the Fricke dosimetry method ii
Table 8: Programmed tests for the second best gas in the Weissler dosimetry experiments by means of the Fricke dosimetry method ii
Table 9: Triiodide production using nitrogen (μmol) iv
Table 10: Triiodide production using argon (μmol) v
Table 11: Triiodide production using air (μmol) vi
Table 12: Ferric ion production using air and argon (μmol) vii

1 Introduction

The average global temperature on earth is increasing year by year[1]–[3] and the human being is the main responsible for it. CO_2 emissions caused by mankind certainly have a strong impact on global warming since this greenhouse gas is being released in great amounts into the atmosphere[4], [5].

In this context, several options are being considered like removing carbon dioxide from the atmosphere. On the one hand, it is being investigated the possibility of storing it (CCS): on the ground, on the sea or just converting it to stable carbonates. The alternative of storing it is the utilization of CO_2(CCU) itself, which implies converting it into useful products as fuel or commercial chemicals like methanol [1].

Nevertheless, a more ambitious alternative to deal with climate change is the prevention of CO_2 emissions per se. Most of carbon dioxide emissions are derived from fossil fuels combustion, indeed, according to recent statistics, fossil fuels represent around 85% (11510 million tonnes of oil equivalent) of the world energy demand [6]. It is then necessary to search new cleaner and sustainable sources of energy, a fact that does not merely imply that the impact of global warming will be reduced but the preservation of our finite natural resources.

In this regard, hydrogen has emerged as the fuel of the future and as an ideal substitute for fossil fuels. It is the most abundant gas in the universe, it has a high specific energy and its combustion is totally clean, although above all, a major reason is its utilization in a fuel cell, which is one of the most efficient technologies to produce electricity nowadays. The way hydrogen is obtained is also an essential key point. In particular, the most widely used method is the reforming of hydrocarbon [7], a process that both contaminates and makes use of fossil fuels. However, there are more available methods like water electrolysis or water sonolysis, being possible to couple both methods simultaneously.

Water electrolysis is a technique where water is “broken” by means of electricity, being decomposed into hydrogen and oxygen. Sonolysis, on the other hand, is produced by means of ultrasound and implies the dissociation of water by different mechanisms from electrolysis. These methods are extremely interesting as the production of hydrogen could be *eco-friendly* if clean energy from renewable sources is used.

The use of ultrasound can certainly play a key role in the future for chemistry and hydrogen production. One of the main effects caused from the application of power ultrasounds to an aqueous solution is cavitation. This physical phenomenon is of great importance as highly reactive radicals are formed and specific conditions of high temperature and pressure are created in the bubbles. Moreover, it has also been demonstrated that power ultrasounds enhance mass transport[7], [8]. Therefore, it is convenient to research and explore the possibilities power ultrasound can provide to hydrogen production and, above all to analyze the parameters that optimize it.

2 Theoretical Background

2.1 Power ultrasound and Sonochemistry

2.1.1 Introduction to Sonochemistry

The purpose of this work is to have a more comprehensive understanding of OH radical formation by means of Sonochemistry.

Sonochemistry is a branch of chemistry that combines chemistry with ultrasound, which, by definition, is the set of pressure waves whose frequency is higher than 20 kHz, that is more or less the upper limit of human hearing. It is important to remark that a distinction is made between two differentiated ranges of frequency.

On the one hand, from 20 to 100 kHz the power transmitted by the waves is high, with, at least, 10 W/cm^2 , being possible to reach 1000 W/cm^2 [9]. This first group is called *Power Ultrasound* and it represents the most interesting range of frequency since these waves influence the medium where they propagate[7], [10] , being able to produce cavitation in a liquid solution. This physical phenomenon is critical in Sonochemistry[7], [8], [11], [12] and it is the main reason that this discipline is focused on this group. On the other hand, approximately from 2 MHz to 10 MHz, it is distinguished a region called *Low Power Ultrasound*. In this case, the power transmitted with the waves is lower than 1 W/cm^2 [9] and there is no effect on the medium of propagation. Some of the main applications of Low power ultrasound are its use for medical purposes and non-destructive testing [10].

Due to certain features discussed below, the application of power ultrasound may improve or change chemical and electrochemical systems. It was precisely in 1934 when Moriguchi [13] for the first time conducted an electrochemical experiment using ultrasound and noticed significant changes in the conversion rates and cell voltages in comparison with silent conditions. Since then, many researches have been undertaken in order to understand and find applications for Sonochemistry[11], [14].

Indeed, several studies suggest the positive effects of ultrasound, just to name a few: Walton et al [15] successfully proved an improvement in hydrogen obtention rate with Platinum electrodes, Budischak et al [16] revealed a considerable improvement in an alkaline water electrolyzer's efficiency and Hagan et al [17] also showed a considerable enhancement of mass transfer sonicating a rotating disk electrode. Another interesting example is the experiments carried out by Durant et al [18], who conducted one of the first tests with sonotrodes and demonstrated a significant enhancement in benzaldehyde and benzoquinone electrochemical reduction.

At present, Sonoelectrochemistry is not just a field of research but a quite developed technology, being employed in different areas such as electroplating, nanomaterials, cleaning, biotechnology, sonoelectroanalysis or sonoelectrosynthesis [12], [19]. Power ultrasound has also been utilized for water treatment successfully, nevertheless, the experiments have been generally carried out at laboratory scale [11].

2.1.2 Phenomena associated to Power Ultrasound

In order to understand the reason behind the beneficial impact of power ultrasound and its repercussions, it is convenient to analyze in depth the phenomena originated by it. Several effects are derived from ultrasonic waves but those that have the most significant impact are acoustic streaming and cavitation [10], [19].

Acoustic streaming or acoustic wind is a process where a macroscopic jet is originated due to the transfer of mechanical momentum from the ultrasonic wave travelling through the liquid. The magnitude of this force relies on different properties such as the absorption coefficient or the amplitude of the ultrasonic pressure [20]. Acoustic streaming can lead to a significant mass transport enhancement, being possible, in some cases, to neglect other effects of power ultrasound [8].

Another major phenomenon involved in Sonochemistry is cavitation and it is the most important event produced by power ultrasound [7], [10], [21]. The nature of the ultrasonic waves makes it possible for negative pressure zones to appear, resulting in the formation and expansion of small bubbles, which, in a matter of microseconds collapse violently [22].This collapse, which is produced at extremely high speed, results in an adiabatic compression, being able to create zones of local temperatures around 5000 °C and 2000 atm [23]. These conditions do not only imply a set of mechanical phenomena but also a chemical alteration in the system. Figure 1 summarizes the main physical effects produced by ultrasound in a liquid solution.

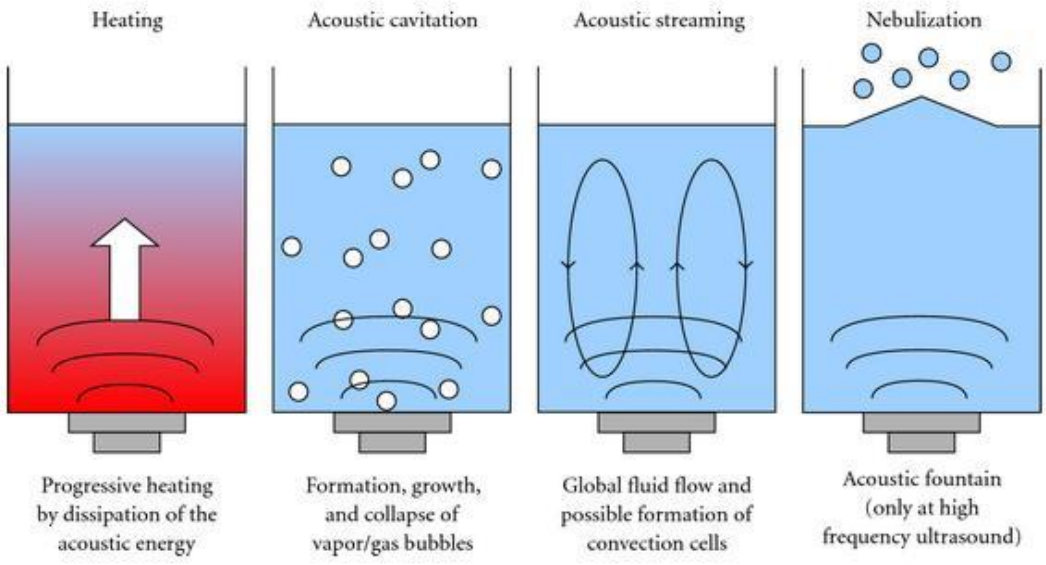

Figure 1: Physical effects produced by ultrasonic irradiation in a liquid solution [10]

Because of the high temperatures and pressures achieved in the implosion of the bubbles, the water undergoes a process called *sonolysis*, where its thermal dissociation occurs, forming different species such as hydrogen or hydroxyl radicals (the most oxidative free radical) [24], the latter being also the most dominating specie [7]. Hydroxyl radical has an oxidizing potential of 2.06 V, which makes it extremely oxidant and capable of reacting with a wide range of particles at constant high rates [25].

Acoustic cavitation also implies a number of physical effects such as microstreaming and turbulence, the formation of microjets or the appearance of shock waves [8], [26]. These processes can strongly affect mass transport and are reported to have more importance at high frequencies, in contrast to acoustic streaming, which is more relevant at lower frequencies [12]. Mass transfer enhancement can be approximately described by the decrease in the diffusion layer thickness and this parameter have a strong impact on electrochemical systems, varying the limiting current, which can be calculated quantitatively if its variation is known [8], [11].For example, making some assumptions it is possible to estimate the limiting current on the basis of the diffusion layer thickness for macrodisk and microdisk electrodes by Eq. (1) [8]:

$$I_{\mathrm{lim}} = \frac{nFDAC_{bulk}}{\partial} \tag{1}$$

Being n the number of electrons, F the Faraday constant, D the diffusion coefficient, A the electrode area, C_{bulk} the concentration of the bulk solution and ∂ the diffusion layer thickness. Mass transfer variation can drastically impact the electrochemical process, being able to change the reaction pathway [8], [27].

Among all these physical effects, the microjets originated near the surface of the electrode have special relevance. This statement seems reasonable since the velocities reached by microjets are around 100 m/s, which, according to Legay et al [10] are considerable higher than the velocities reached by means of acoustic streaming or microturbulence, a fact that has also heat transfer implications. Furthermore, Klima et al [26] confirmed that both acoustic streaming and microjets were able to enhance mass transport, however, microjets were particularly interesting as they could also clean and activate a passivated-electrode, in contrast to acoustic streaming.

The positive impact of cavitation in this aspect, however, could also bring negative effects as it has been reported the appearance of erosion phenomena, particularly relevant when a long-term and high power is applied coupled with a short distance between the electrode and the transducer [8]. The damaged caused to the electrode could decrease the efficiency of the reaction, moreover, it is important to note that cavitation can also affect the surface of the transducer, resulting in the contamination of the electrochemical process, with its corresponding negative implications, including the efficiency decrease of the sonotrode [11], [28].

2.1.3 Ultrasound systems

There are different types of equipment that produce ultrasound, being electromechanical apparatus as ultrasonic bath and ultrasonic horns the most commonly used systems (Figure 2).

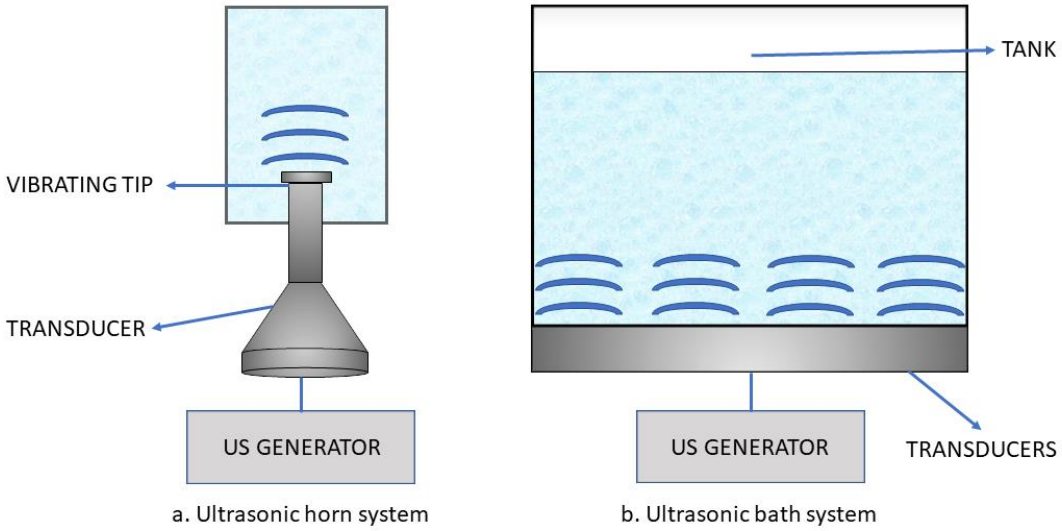

Figure 2: Ultrasonic horn and ultrasonic bath schemes

Ultrasonic bath is well known for its simplicity and low price. It consists of a tank (generally made with stainless steel) with transducers attached to the base and the power is distributed equally through the cell walls. The main problem with ultrasonic baths is its limited power (1-2 W/cm^2) and the fact that, generally, this kind of systems only operate at a fixed frequency [29]. It is also important to design the reaction vessel taking into account that the ultrasonic waves are emitted vertically from the base of the tank, for instance, spherical vessels are not recommended. The shape of the vessel is important, but it is also important to consider its position in the bath and the liquid height itself, as these parameters affect the power the cell receives.

If a higher power is required, the best solution is to use an ultrasonic horn instead. In these devices, the ultrasonic power is directly applied at the tip of the horn, resulting in a much higher and localized power (10-1000 W/cm^2) [11] than in ultrasonic bath systems. If the ultrasonic horn is used concurrently as working electrode it is called "sonotrode", however the term sonotrode is commonly used to refer to the transducer itself. Although ultrasonic waves are generated in an ultrasound generator, ultrasonic probes, far from being a meaningless piece, have a very important role in the final transmitted power. Precisely, the horn amplifies the vibration of the transducer [29], being its shape an important factor that affects the resulting ultrasonic power.

In this respect, Fang et al [19] investigated with Particle Image Velocimetry and the Weissler dosimetry the impact of the horn tip shape in cavitation and acoustic streaming. They concluded that the shape of the tip strongly affected acoustic streaming and, to a lesser degree, cavitation, which resulted to be influenced by other factors as the vibration amplitudes.

An interesting approach to calculate approximately the amplitude of the pressure produced by ultrasonic waves on the axis of a flat and cylindrical horn is given by Eq. (2) [20]. Specifically, λ represents the wavelength of the wave, *x* stands for the distance from the tip and *r* is the radius of the tip itself. It is assumed that there are no reflections from the wall.

$$p = \sin\frac{\pi}{\lambda}\left[\sqrt{(x^2 + r^2)} - x\right] \tag{2}$$

This expression provides a reasonable understanding of how the pressure distributes through the axis of the horn; however, it does not consider that a large proportion of energy is lost due to cavitation. As a result, if power ultrasound is used and cavitation is possible, the amplitude of the pressure will decrease faster and cavitation will only occur near to the tip.

The material of the horn is also important as it is meant to resist the erosion effects produced by cavitation, moreover, it should resist several chemical environments as direct contact with the solution is frequently required. Because of its capacity to overcome these imposed restrictions, coupled to the fact that it has a very low acoustic loss, titanium alloy is generally used. Nevertheless, the horn will have to be replaced eventually due to deterioration, in Figure 3 can be observed an ultrasonic horn after several weeks of use. The main disadvantages of ultrasonic horns are related to the fact that the operating frequency is fixed, and that some contamination may occur in the sonicated solution from the erosion produced at the tip.

Figure 3: Erosion effects observed in an ultrasonic horn made with titanium

2.2 Power ultrasound and hydrogen production

Hydrogen is the most abundant and simplest element in the universe, without it, life would not be possible. It is not only a critical element because of the fact that it is part of many essential chemical compounds (including proteins or carbohydrate) but because our society is entirely dependent on it. For instance, large amounts of hydrogen are necessary in order to synthesize ammonia (one of the most produced chemicals in the world), hydrochloric acid or methanol. Besides being important for the chemical industry, it is also a crucial element in different areas such as the food industry, the aerospace industry or in the production of heavy water for nuclear plants, for instance.

The applications of hydrogen are certainly numerous, furthermore, this last decade hydrogen is emerging as the perfect substitute of fossil fuels. In fact, it may not only be used as a clean fuel in internal combustion engines, achieving higher efficiencies than those powered with fossil fuels, but as an energy vector to generate electricity by means of fuel cells. Fuel cells are arising as the perfect source of energy for electric motors, they can provide electricity with good efficiencies in a clean way as long as the hydrogen used is also obtained cleanly and sustainably.

Indeed, it is possible to produce hydrogen with electricity from renewable sources, for example, by means of water electrolysis, and, although it is still an expensive technology, the prices of electrolyzers (devices in which electrolysis is carried out) are expected to decrease over time [30]. Another way to produce hydrogen cleanly from water is by means of power ultrasound and, although this innovative technology is currently under development, it seems very promising and convenient as it can also be used together with water electrolysis.

2.2.1 Mechanisms of sonochemical production of hydrogen

The application of power ultrasound into a liquid leads to the growth and violent collapse of minute bubbles adiabatically (known as acoustic cavitation) [31], being essentially composed of gases and water vapor dissolved in the fluid [32]. This event, as mentioned above, creates extreme and unique conditions of local high temperatures and pressures that are responsible for the thermal disassociation of water vapor and other gases trapped in the bubble into reactive radicals such as $H^{\cdot}$ or $^{\cdot}OH$ [32], [33]. These reactive species are highly unstable and may react forming hydrogen, which is the main product of this process [7], [34].

The production of hydrogen takes places through two different ways (Figure 4): It is synthesized in the gas phase of the bubble by Eq. (3) and there is also some yield at the bubble wall by means of recombination of hydrogen radicals (Eq. (4)) , moreover, it is still controversial which of the two is the main source of Hydrogen [7], [34].

$$H \bullet + \bullet OH \leftrightarrow H_2 + O \quad (3)$$

$$H \bullet + H \bullet \leftrightarrow H_2 \quad (4)$$

According to Merouani et al [34], who performed a numerical simulation combining dynamics of single acoustic bubbles and chemical kinetics, concluded that the main mechanism of hydrogen produced is the reaction taking place at the gas phase of the bubbles (Eq. (3)). The results of the research showed a considerable difference between the two mechanisms, specially at 20 kHz, where the reaction at the gas phase created more hydrogen by a factor of 7,22.

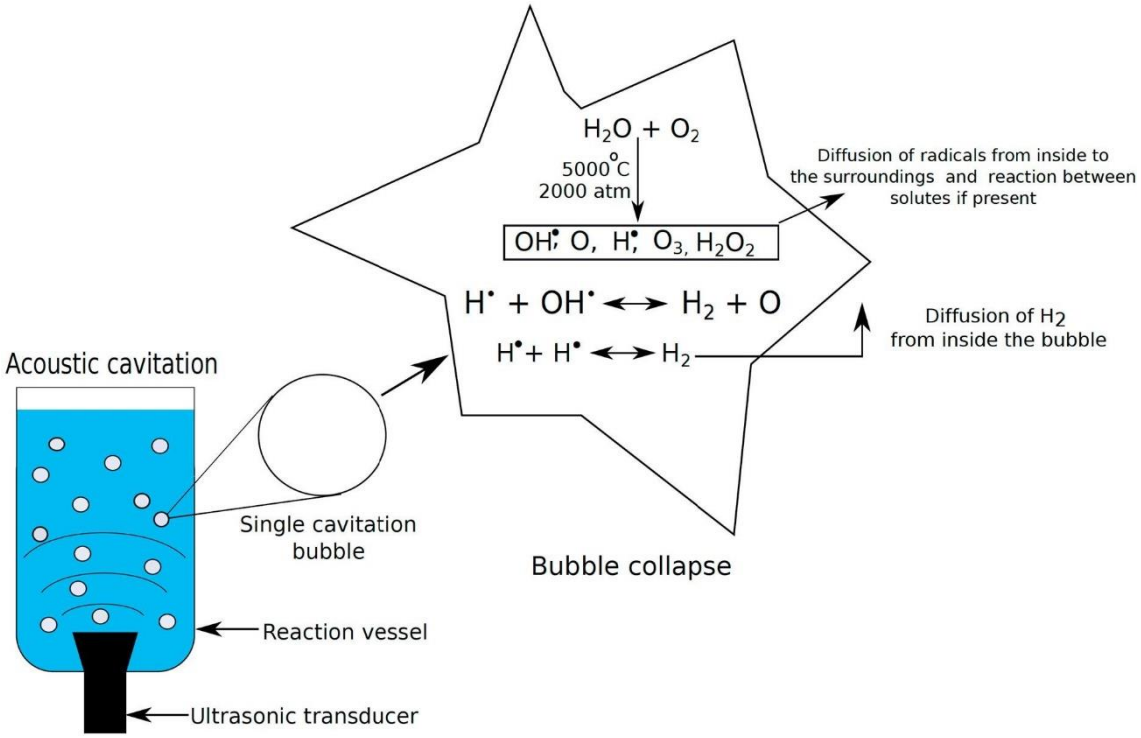

Figure 4: Production of hydrogen by acoustic cavitation [7]

Therefore, it seems reasonable to assume that the more the concentration of $H^{\cdot}$ and $^{\cdot}OH$, the higher the production rate of hydrogen will be. This statement is, in fact, consistent with the findings of Merouani et al [34], [35]. It is then necessary to fully comprehend acoustic cavitation phenomena and the parameters affecting the bubble population, which is the ultimate cause of the formation of reactive species.

It is important to add that not every bubble is interesting in terms of sonochemical activity. There are two main groups of bubbles generated by acoustic cavitation [34], [36], [37]; stable/non-inertial and transient/inertial bubbles. The difference between the two groups is mainly that stable bubbles last over many cycles and oscillate steadily, while transient bubbles are unstable, growing uncontrollably until they collapse fiercely.

This collapse brings to the fragmentation of the bubble, which either creates tiniest bubbles or it is just dissolved in the solution. These small bubbles enhance the

interaction between the bubble surface and the solution, making the greatest contribution to sonochemical effects [38]. The bubbles that produce sonochemical effects are called active bubbles [34] and they belong to this second group.

It is also possible to establish a broader classification of bubble population. For instance, Yasui [39] distinguishes between 4 categories of bubbles that grow by means of rectified diffusion, being two of them bubbles that emit light (stable and unstable sonoluminescing bubbles) and the other two, bubbles that do not emit light (unstable and degas bubbles). Rectified diffusion stands for the growth experimented by bubbles due to the pressure caused by ultrasound and, together with coalescence (the combination of two bubbles), constitute the mechanisms by which bubbles grow in a sonicated environment [40].

Before going into detail regarding the main factors that affect bubble population, it is important to define the ambient radius, which is the radius of a bubble when it is not being irradiated by ultrasound [41]. This parameter, as well as other factors as acoustic amplitude or frequency, defines the type of the bubble that will be formed [39].

2.2.2 Parameters that affect sonochemical activity

Several factors are involved in the formation of active bubbles and they are related to the ones that affect the bubble surface instability [38].

2.2.2.1 Frequency

One of the most important parameters is precisely the ultrasonic frequency, which affects the amount of bubbles created, their size, distribution and sonochemical activity [32], [35], [38]. Koda et al [42] concluded that the optimal frequency is around 300 kHz, while other publications suggest that the optimum is around other values like 355 kHz [34]. However, it is not clear which is the best frequency since its increase have positive and negative effects.

Regarding the size of the bubble, according to Brotchie et al [43], increasing ultrasonic frequency results in a smaller mean size of the bubble. This statement is also supported by Merouani et al [32], who studied the optimal ambient radius regarding hydrogen production for different frequencies, concluding that the optimum bubble radius, along with its range, decrease with an increase of the ultrasonic frequency. Hence, while at lower frequencies bubbles are larger, collapsing violently and experiencing instability quickly, coalescence also increases, bringing negative effects as degas bubbles (which are not active) can be formed [38], [44]. At higher frequencies, bubbles can also experience coalescence due to antinode regions proximity, however, in this case it could bring positive effects as tiny inactive bubbles could become large enough to be active bubbles, furthermore, at higher frequencies, bubbles are subject to more instabilities [38].

It is important to note that at higher frequencies, the collapse time is shorter, decreasing the obtention of reactive species and the production of hydrogen [35]. In conclusion, the optimal frequency is a compromise between high and low frequencies.

2.2.2.2 Liquid temperature and bubble temperature

The liquid temperature is also an important factor to consider and, as with ultrasonic frequency, there is an optimal value that optimizes the production of hydrogen, which depends on many variables. According to Yasui et al [45], who carried out a numerical simulation with different amplitudes and ambient pressure, concluded that there is an optimum bubble temperature that enhances free radical obtention rate. For example, for air bubbles and regardless of the pressure, an optimum temperature of about $5500\ \mathrm{K}$ was estimated. More recently, Merouani et al [46] conducted computer simulations for oxygen and argon bubbles with different models, finding an optimum temperature for the production of $^{\cdot}OH$ radicals about 5200 K in the case of oxygen. They also found an optimal temperature for argon bubble, revealing a dependence between the frequency and the optimal bubble temperature, being 5200 K at 20 kHz but decreasing to 4200 K at 355 kHz [37]. In this last study, the liquid temperature was varied from 20 °C to 50 °C, finding an optimal value of 30 °C.

Precisely, the bubble temperature and the liquid temperature are connected. An increase in in the liquid temperature raises the vapor pressure, which results in a higher amount of water vapor trapped in the liquid, which could be beneficial for the sonochemical activity as reactive species are formed by it, however, higher temperatures also decrease the polytropic index and the gas solubility, which reduces free radical formation and cavitation nuclei respectively [35]. Furthermore, an increase of water vapor can also cushion the collapse of the bubble, reducing the peak temperature and the sonochemical activity [38].

2.2.2.3 Dissolved gas

Another key factor, which is also related to temperature and frequency is the gas saturation effect. It is possible to relate the polytropic index of the gas and the bubble radius with its collapse temperature (Eq.(5)) [47], an important parameter that, as it has already been showed, affects the production of reactive species. On the other hand, the thermal conductivity of the gas is important as well, impacting the heat dissipation of the bubble and thereby the collapse temperature too [7], [47].

$$T_{collapse} = T_0 \left(\frac{R_{max}}{R_{collapse}} \right)^{3(\gamma-1)} \tag{5}$$

One interesting fact about the gas saturation effect is that it is also affected by frequency, furthermore, Merouani et al [35] found that at lower frequencies the impact of the dissolved gas was far less important than at higher frequencies. This was believed to be linked to the fact that at low frequencies most of the content of the bubble is water vapor. The impact of the ultrasonic frequency on different saturation gases was also reported by other authors like Dalodiere et al [48].

2.2.2.4 Ultrasonic intensity and other parameters

The power emitted by the transducer is of fundamental importance. Ultrasonic intensity enhances indirectly the production of reactive species since an increase in this parameter increases both the collapse temperature and the amount of water vapor trapped in the bubbles, being these effects seemingly more relevant at higher frequencies. Furthermore, high ultrasonic intensities can increase the collapse time [7]. Hence, a higher ultrasonic frequency results in a higher sonochemical activity.

There are other factors affecting the sonochemical production of hydrogen such as the liquid height of the solution, the addition of surfactants, the type of transducer used, the PH, the viscosity, or the configuration of the reactor, just to name a few. It has become apparent that there are many parameters involved in the formation of free radicals and the fact that all of them constitute a very complex system.

2.3 Dosimetry methods

In order to measure the amount of reactive species formed by acoustic cavitation, it is necessary to perform a dosimetry study, which also provides an order of magnitude about the ultrasonic radiation received by the solution. As it has been mentioned above, the radicals involved in the sonochemical production of hydrogen are mainly $H^{\cdot}$ and $^{\cdot}OH$. These particles are very unstable and react easily with other particles, as a result, they vanish in a short period of time, being difficult to measure them.

In this regard, chemical dosimetry methods make use of different chemicals that react with these free radicals, producing a new and stable chemical compound, which amount can be related to the number of radicals formed during sonication. A wide variety of methods are used but it is worth highlighting among them the Weissler and the Fricke dosimetry for their reliability and simplicity, although the sensitivity achieved by these methods is limited [49].

2.3.1 Weissler dosimetry

This dosimetry method represents one of the most widely used methods available to quantify $\cdot OH$ production rate due to its simplicity [50]. It is also known as potassium iodide dosimetry since the iodine ions of a potassium iodide solution react with hydroxyl radicals, forming triiodide after various steps. Therefore, the only element required to use this method is a solution of potassium iodide and a UV-spectrophotometer.

The process begins when a hydroxyl radical oxidizes an iodide ion, it is formed an iodine atom (Eq. (6)). The iodine atom reacts with the iodine ion forming $\cdot I_2^-$ (Eq. (7)), which decay synthesizing iodine (Eq. (8)), which in turn reacts with another iodine ion forming triiodide (Eq. (9)) [49].

$$\bullet \mathrm{OH} + \mathrm{I}^- \rightarrow \mathrm{OH}^- + \mathrm{I} \bullet \tag{6}$$

$$\mathrm{I} \bullet + \mathrm{I}^- \leftrightarrows \mathrm{I}_2^- \bullet \tag{7}$$

$$2\ \mathrm{I}_2^- \bullet \rightarrow \mathrm{I}_2 + 2\ \mathrm{I}^- \tag{8}$$

$$\mathrm{I}_2 + \mathrm{I}^- \leftrightarrows \mathrm{I}_3{}^- \tag{9}$$

It is important to add that the yield of iodine could decrease as it could react with hydrogen atoms by Eq. (10), impacting this way the obtention of triiodide. Furthermore, superoxide radical can also affect the amount of iodine by Eq. (11) [51].

$$\mathrm{H} \bullet + \mathrm{I}_2 \rightarrow \mathrm{HI} + \mathrm{I} \bullet \tag{10}$$

$$\mathrm{O}_2^- \bullet + \mathrm{I}_2 \rightarrow \mathrm{O}_2 + \mathrm{I}_2^- \bullet \tag{11}$$

The triiodide formation can be easily measured by means of a UV-Spectrophotometer at a wavelength of 350 nm[49]. It is possible to calculate the concentration of the formed triiodide by means of the Beer-Lambert law, which relates the absorbance to the concentration of a specie. The molar linear extinction coefficient Ɛ for triiodide is $25000\ l/mol \cdot cm$ [52].

2.3.2 Fricke dosimetry

Another important dosimetry method used in sonochemistry is the Fricke dosimetry or ferrous sulfate dosimetry, due to the utilization of this chemical compound. It is one of the most useful dosimeters, however, it has also some disadvantages like the fact that it has a high sensitivity to impurities, affecting the yield of ferric ion, the particle measured with this method [53]. Another disadvantage of the Fricke dosimetry is its limited dose range from 40 to 400 Gy [54], being Gy the derived unit of ionizing radiation dose in the International System of Units, equivalent to 1 J / 1 kg.

The solution employed to perform this dosimetry method consists of three different chemical compounds diluted in purified water: $(NH_4)_2Fe(SO_4)_2 \bullet 6\mathrm{H_2}O$ $(0{,}001\ mol/l)$, H_2SO_4 $(0{,}4\ mol/l)$ and $NaCl$ $(0{,}001\ mol/l)$. The formation of Fe^{3+} is produced by means of Fe^{2+} oxidation, which occurs due to the interaction with both hydroxyl radical and hydrogen peroxide (Eq. (12) and Eq. (13))[51].

$$\bullet \mathrm{OH} + \mathrm{Fe}^{2+} + H^+ \rightarrow \mathrm{H_2}O + Fe^{3+} \tag{12}$$

$$\mathrm{H_2O_2} + \mathrm{Fe}^{2+} + H^+ \rightarrow \mathrm{H_2}O + Fe^{3+} + \bullet \mathrm{OH} \tag{13}$$

In order to quantify the production rate of Fe^{3+} it is possible to use a Uv-spectrophotometer at a wavelength of 204 nm, bearing in mind that its molar extinction coefficient Ɛ is $2197\ l/mol \cdot cm$ [53].

2.3.3 Other dosimetry methods

In addition to the Fricke and Weissler dosimetry, it is possible to quantify the formation of free radicals by other methods such as electron spin resonance, nitrous and nitric acid formation, porphyrin decomposition or Terephthalate dosimetry [55], [56], just to name a few. There also exists other alternatives to chemical dosimetry methods. For example, it is possible to quantify approximately the formation of radicals with an erosion sensor or with chemiluminescence methods [56].

Amongst these techniques, Terephthalate dosimetry is probably the most known and interesting one. Starting from a terephthalic acid solution, hydroxyl radicals react with it forming hydroxyterephthalic acid, which unlike terephthalic acid, has fluorescent properties, emitting at a wavelength of 323 nm [56]. Therefore, this technique allows to measure the formation of radicals achieving a high sensitivity [57], furthermore, it is a simple and cheap dosimetry method [56]–[58].

3 Materials and Methods

3.1 Experimental setup and materials

The setup includes mainly an ultrasound generator, a reactor cell, a thermostatic bath, a pump, a valve and some other component that will be described below.

The ultrasound generator is a Hielscher UP400St with a working frequency of 24 kHz and a maximum power of 400 W. A S24d22D sonotrode (Ø 22 mm) made of titanium is attached to the ultrasonicator. Embedded to the ultrasonicator is the Besançon cell (Figure 5), an especial designed microsonoreactor made of glass that contains the sonicated solution. It is composed of two chambers: The cooling water chamber and the reactor cell, which is isolated from the cooling water circuit. Since the solution is not sonicated directly some power is lost in the process, however, the separation of the cell is necessary in order to regulate its temperature. Furthermore, this system prevents the solution from being contaminated by the eroded titanium of the ultrasonic horn. The distance between the probe and the reactor bottom is 15 mm.

Figure 5: Besançon microsonoreactor (15 mm)

In order to saturate the solution with different gases and avoid the air to come inside, a special cap was designed. This element seals the reactor chamber and it is composed of 5 holes of which only 3 are used. One hole is required to pour the solution into the reactor, another one to inject the saturation gas and a third hole is required to connect the gas bubbler, an element that keeps the reactor cell isolated from the external air (Figure 6).

Water loop, pump and thermostatic bath make up the temperature control system. Furthermore, a valve is installed in series in the water loop system in order to pressurize the recirculated water in the reactor. It is important to overpressurize the loop water, this way less cavitation is produced, and more ultrasonic radiation reaches the solution.

The pumping system is a Self-priming gear pump from Biltema. A Power supply was needed in order to power the pump, specifically, an EA-PS 5040-40 A model was used. The thermostatic bath regulates the temperature and it is used a Neslab RTE-221 model.

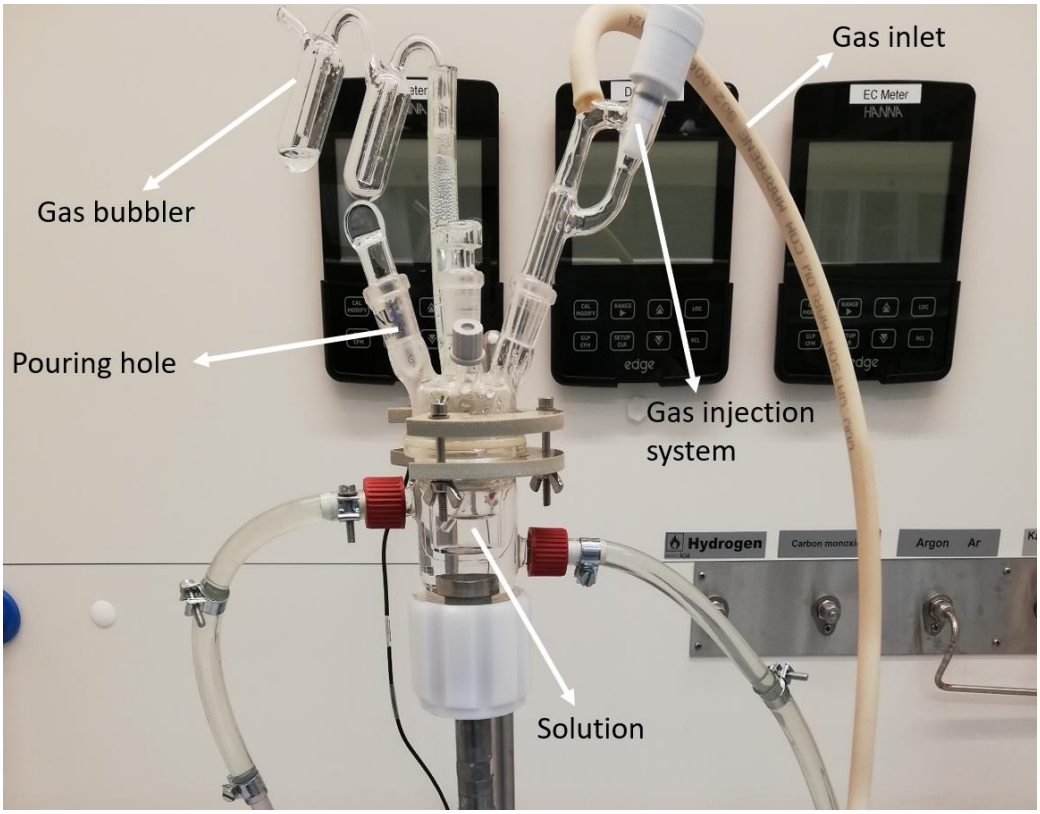

Figure 6: Main elements of the cell

The saturated gas mass flow was the same for the three gases as a precision gas mass flow controller was used (Alicat MC-Series). The mass flow was adjusted at 250 standard cubic centimeter per minute.

The samples were analyzed by means of two different spectrophotometers. For most of the Weissler dosimetry tests, Thermo Scientific GENESYS 30 visible spectrophotometer (325-1100 nm) was used. UV-Visible Spectronic Helios Gamma spectrophotometer (190-1100 nm) was utilized for all the tests of the Fricke dosimetry and a few of the Weissler dosimetry. The cuvettes were supplied by VWR and are made of polymethyl methacrylate, with a standard lightpath of 1 cm.

The device DO kit Multiparameter Meter edge was utilized to measure the dissolved oxygen in the concentration in order to calculate approximately the time needed to saturate the solution. A DO-ZERO solution provided by Thermo Scientific was used to calibrate the DO meter.

Regarding the chemicals used, ammonium iron (II) sulfate hexahydrate and potassium iodide were acquired from Sigma-Aldrich. Sulfuric acid was acquired as an aqueous solution with a molarity of 4 mol/l from VWR. The volumetric flasks used to prepare the solutions are made of borosilicate glass and all of them are class A, in accordance with DIN EN ISO 1042. The tolerance of the flasks utilized in the experiments is shown in Table 1. An overview of the setup is shown in Figure 7.

Table 1: Tolerance and relative errors of the flasks employed

Graduated Flasks	Tolerance	Relative error (%)
5 ml	±0,04 ml	0,8
50 ml	±0,06 ml	0,12
100 ml	±0,1 ml	0,1
200 ml	±0,15 ml	0,075

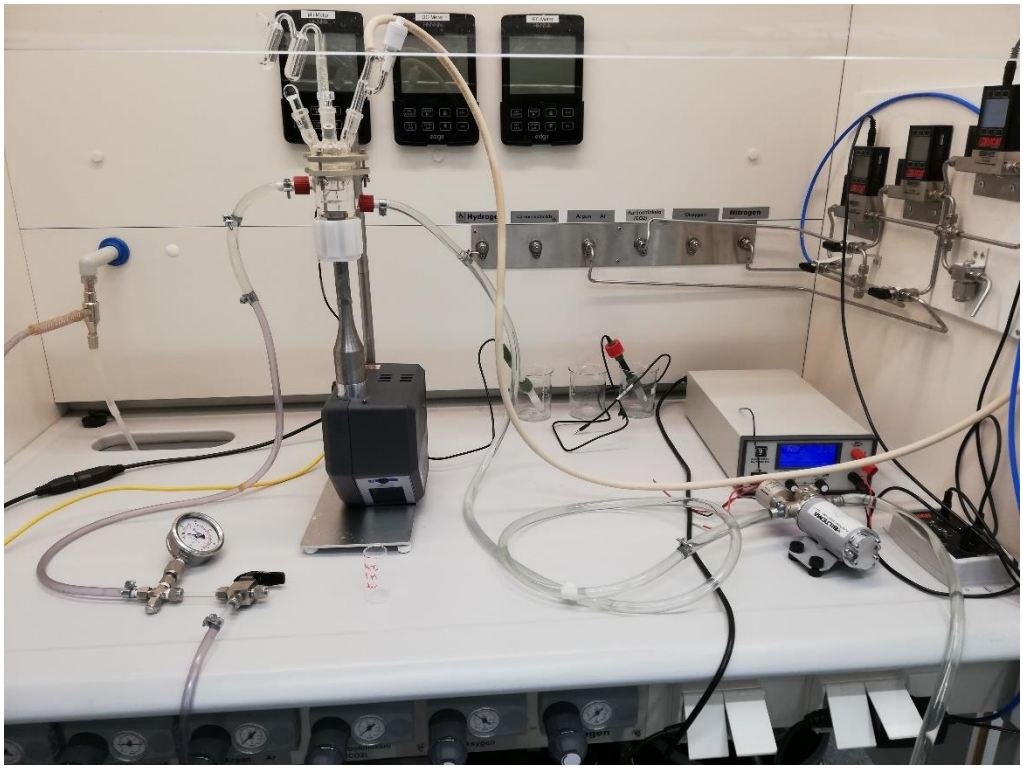

Figure 7: Overview of the setup

3.2 Experimental procedure

Three different parameters were analyzed with the purpose of analyzing their impact on OH radical formation, which was characterized by means of two different dosimetry methods (Weissler and Fricke only for the first two parameters):

- Effect of a dissolved gas: Air, nitrogen and argon
- Effect of Temperature: Different initial temperatures (10 °C, 20 °C, 30 °C, 40 °C)
- Effect of the solution concentration: Different concentrations of potassium iodide were tested when the Weissler dosimetry method tests were carried out (0.1 M, 0,4 M,0.7 M, 1M)

Every test was repeated 3 times in view of improving the reliability of the results. A more detailed description about the experimental plan can be seen in Appendix A. The experimental procedure was almost the same for the two dosimetry methods and it is explained below:

The first step was to prepare the solution. The amount of chemicals depended on the dosimetry method and the concentration tested (for the Weissler dosimetry) besides the flask used to prepare the solution. For example, in Table 2, it is explained the quantity required of chemicals in terms of mass for every experiment, assuming that everything is mixed in a 200 ml flask. Other flasks were needed throughout the experiments, but this was the most commonly used.

Table 2: Mass of chemical compound needed for each test using a 200 ml flask

	Mass of product (g)			
Weissler dosimetry	Potassium iodide	Salt	Sulfuric acid	Ammonium iron (II) sulfate hexahydrate
0,1 M	3,32	-	-	-
0,4 M	13,28	-	-	-
0,7 M	23,24	-	-	-
1 M	33,2	-	-	-
Fricke dosimetry	-	0,0117	8,173	0,0784

After preparing the solution, a flask containing 5 ml of it was poured into the reactor and the corresponding gas was injected through the injection bubbler. This constant flow of gas in form of bubbles saturated the solution. In order to get a sense about the time needed to saturate the solution, a DO meter was used along with a beaker with similar characteristics to the Besançon cell. The results of the tests can be seen in Appendix B and it shows the time required to remove oxygen in the case of argon and nitrogen and the time to saturate the solution with air (a plateau is reached). The saturation of air takes less than 2 minutes as it is almost saturated from the beginning. Argon and nitrogen lose all the oxygen around 6 minutes and 30 seconds. It was decided to saturate the solution for 10 minutes to ensure that the gas was saturated.

While the solution is being saturated by the gas, the thermostatic bath keeps the water temperature and the pump recirculates the water from the thermostatic bath to the reactor. This pumping is required since the solution gets the specific temperature by heat transfer through the wall that separates both chambers. A thermocouple was used to measure the required time needed to reach the working temperature in the reactor cell. In the worst-case scenario, the time was less than 5 minutes. Accordingly, the pump was turned on for 6 minutes before the start of the test

The pump has also an important role in the results as it enhances the formation of reactive species in the reactor cell. In fact, it was originally intended to conduct the experiments without any additional pump as the Neslab RTE-221 thermostatic bath included a small pump inside to recirculate the water. However, the water loop circuit absorbed too much energy, thus drastically decreasing the ultrasonic power received by the solution into the microsonoreactor. It has been mentioned above that cavitation absorbs great amounts of energy. In this case, the acoustic cavitation produced in the reactor cell before pressurizing the recirculating water was almost nonexistent.

With the aim of avoiding energy losses by acoustic cavitation in the cooling chamber and therefore increasing the energy received by the solution in the reactor chamber, it was decided to pressurize the recirculated water, and this required a more powerful pump. An overpressure of 1,5 bar was designated for all the experiments. The regulation of the pressure was conducted using a little valve and a manometer.

An initial test shown in Figure 8 was conducted using the Weissler dosimeter. A solution of 0,1 mol/l potassium iodide was prepared and poured both into the reactor and the thermostatic bath. This test proved that the production of radical species was drastically increased by pressurizing the water loop circuit. Furthermore, it was found that whereas the radical formation in the water loop was limited it was not negligible.

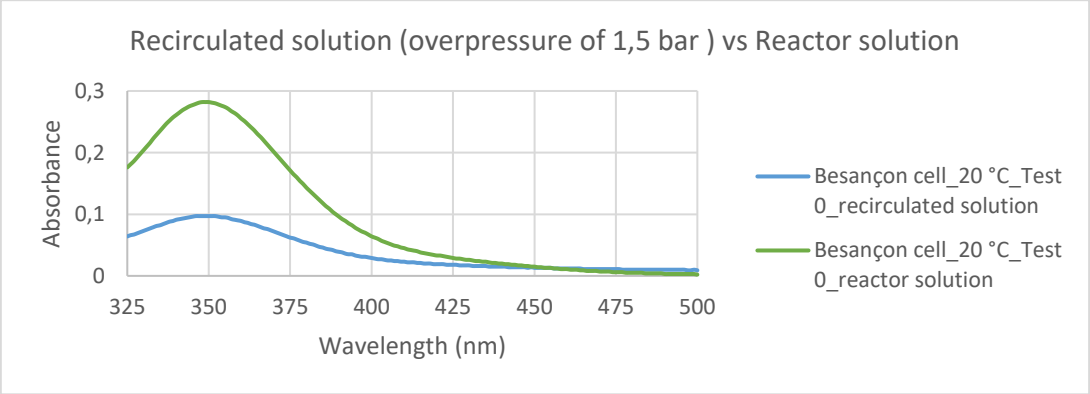

Figure 8: Comparison between the pressurized recirculated solution and the cell

Once the solution was saturated with gas and it reached the working temperature, the ultrasound generator was turned on. The time of sonication was 5 minutes for every single test.

Following the completion of each test, the reactor was cleaned at least three times with deionized water. A simple scheme on the operation during sonication is shown in Figure 9. It is important to add that the number of experiments per day at 40 °C had to be reduced to 1 as the transducer became too hot.

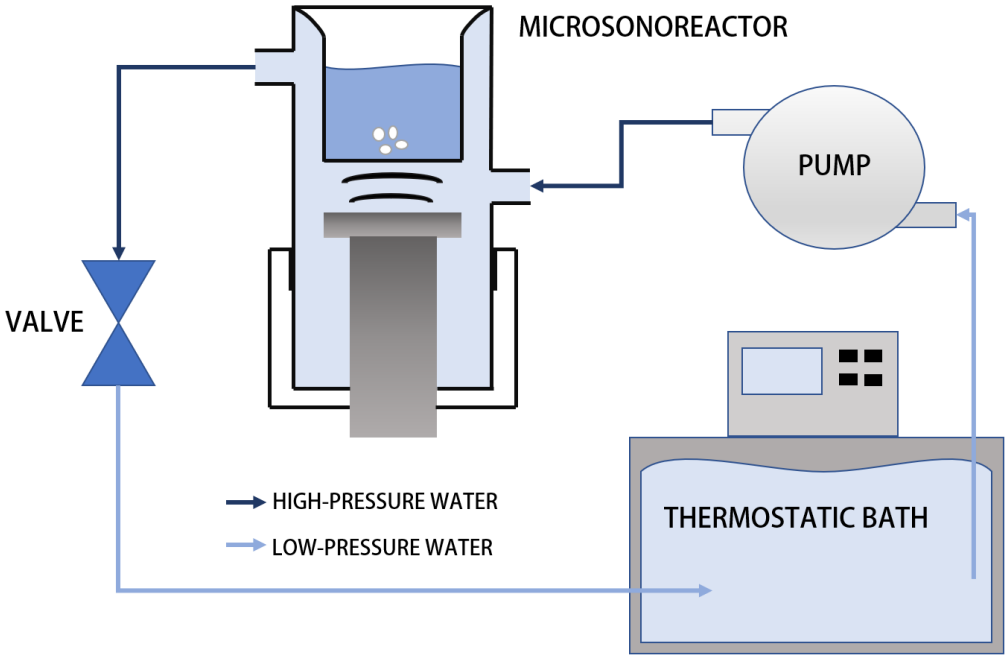

Figure 9: Functioning scheme about the experimental setup during sonication

Once the solution was sonicated for 5 minutes it was extracted from the microsonoreactor using a pipette. Normally, Genesys 30 spectrophotometer was used in order to characterize radical formation on potassium iodide samples (Weissler dosimetry), but at the end of the experimental plan it malfunctioned so the spectrophotometer assigned to the Fricke dosimetry tests had to be used instead. Spectronic Helios Gamma spectrophotometer is older than Genesys 30, however, it has a broader range of wavelength as Genesys 30 minimum wavelength is 325 nm while Spectronic Helios Gamma operates between 190 and 1100 nm.

The concentration of radicals was easily calculated using Beer-Lambert law Eq.(14):

$$c = \frac{A}{\mathrm{E} \cdot l} \tag{14}$$

Being A the absorption coefficient (given by the spectrophotometer), E the molar extinction coefficient (l/mol·cm) and l the cuvette lightpath (1 cm standard length in our case). As mentioned above, the molar extinction coefficient of triiodide at 350 nm is 25000 l/mol·cm while the molar extinction coefficient of ferric ion at 204 nm is 2197 l/mol·cm.

The samples were analyzed instantly after the experiment, except for the ones that should be analyzed in Helios Gamma spectrophotometer, which was located in another different building.

A zero-base sample was extracted for each test in order to improve the accuracy of the results. Figure 10 shows an example of the last samples tested during the Weissler dosimetry, which were analyzed with UV-Visible Spectronic Helios Gamma spectrophotometer as Genesys 30 spectrophotometer stopped working in that period of time.

Figure 10:Testing of samples with Helios Gamma spectrophotometer

3.3 Major setbacks

Throughout the experiments, several problems had to be addressed. Indeed, the fact of working with pressurized water caused multiple issues, specially at 40 degrees. During the first days, when low temperatures were tested, the microsonoreactor performed properly. Nevertheless, when the tests at 30 degrees began, the cap attached to the Besançon cell eventually slipped and opened. As a consequence, great amounts of water suddenly started to leak.

At 30 degrees some tests could be done, however, when the temperature was set at 40 degrees, most of the time this event happened, making impossible to take a valid sample. Making some adjustments in the silicon that sealed the cap made possible to obtain the first data at 40 degrees, but the leaking still happened occasionally. This problem caused a big delay in the schedule as each time it happened the reactor had to be dissembled and a new solution had to be saturated with gas for 10 minutes again. This problem wasn't solved until a new cap was bough and small additional measures were taken. Working at high temperatures resulted to be challenging, not only because

of the sudden leaking, but because the transducer heated up in excess, being at some points difficult to continue the tests as the transducer didn't work nominally.

Another big issue happened with the cap at the end of the tests. While an experiment at 40 degrees was taking place with the Fricke dosimetry, the cap suddenly cracked, and a large amount of water leaked (Figure 11.b) . It is believed that this happened due to some minor leaking of sulfuric acid into the thread of the cap when the solution was being poured into the reactor. This event marked the end of the experiments as new material had to be bought and the time available was limited. A new and more resistant cap made with teflon was ordered.

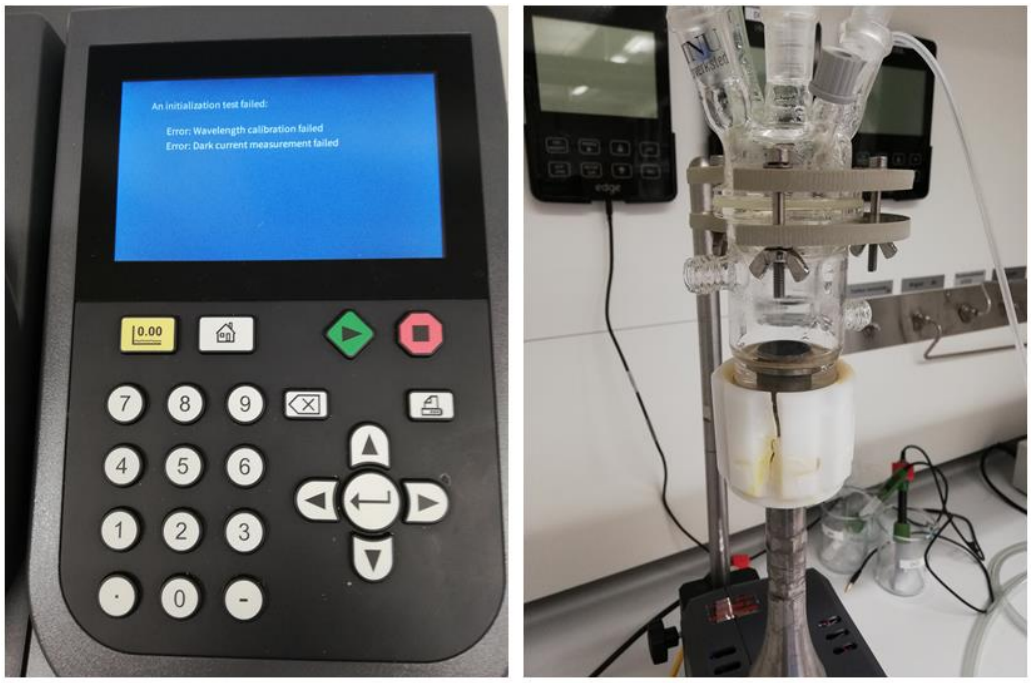

a. Error messages from the spectrophotometer

b. Broken cap during a Fricke dosimetry test

Figure 11: Some of the issues experienced during the experiments

The water loop system was another source of problems. Even though it performed properly most of the time, tiny droplets leaked occasionally at one of the pipe junctions, specially at the connections with the microreactor. But not every issue was related to the set up. At some point Genesys 30 spectrophotometer suddenly began to malfunction (Figure 11.a). After several unsuccessful attempts, it was decided to use the old spectrophotometer assigned to the Fricke dosimetry tests. Delays in the delivery of chemicals or equipment also adversely affected the time schedule of the tests. Furthermore, at certain times, some fragile pieces broke, being necessary to wait for the glassblower to repair them. The preparation of the set up was also a time-consuming matter.

4 Results and Discussion

The results of the experiments performed in the course of this work are presented in this section. For the Weissler dosimetry method, it was analyzed the effect of potassium iodide (KI) concentration, the effect of three different dissolved gases (nitrogen, argon and air) and the effect of the initial solution temperature on the formation of triiodide (I_3^-), which is a parameter strongly related to OH radical formation (Eq. (6)- Eq. (9)) . It is also important to mention that, although the water loop temperature was controlled by means of the thermostatic bath, maintaining the temperature inside the reactor cell was unattainable as the heating effects resulting from power ultrasound were stronger than the heat transfer between the reactor cell and the cooling water. In addition, the temperature of the water loop also increased slightly despite of the thermostatic bath cooling effect. However, both the temperature of the water loop and the solution temperature, only moderately increased for every dissolved gas.

An additional experiment was considered in order to test the effect of the water loop overpressure on free radical formation. These tests were conducted by means of potassium iodide with a concentration of 1 molar and using air. This combination was selected as it resulted to be the most effective one in the Weissler dosimetry tests.

Regarding the Fricke dosimetry, ferric ion production was measured to evaluate OH formation (Eq. (12)). Only the two most effective gases in the Weissler dosimetry experiments were tested. Furthermore, the concentration of the initial chemical compounds was not varied, being the solution: $(NH_4)_2Fe(SO_4)_2 \bullet 6H_2O$ $(0{,}001\ mol/l)$, H_2SO_4 $(0{,}4\ mol/l)$ and $NaCl$ $(0{,}001\ mol/l)$. In spite of the fact that all the temperatures were analyzed, two of the three programmed tests at 40 °C with argon were cancelled since some pieces of the set up were critically damaged after a violent decompression.

The amount of triiodide and ferric ion is calculated with Beer-Lambert law, using the proper molar extinction coefficient and taking into account that the volume of the solution was 5 ml for every test. The results extracted from the experiments, as well as the standard deviation and average are shown in Appendix C.

4.1 Weissler dosimetry

4.1.1 Nitrogen

The effect of KI concentration on the averaged triiodide production can be seen in Figure 12. It is possible to observe a direct correlation between the concentration of KI and the production of triiodide. This effect is only different in two averaged points, nevertheless, one point presents a high standard deviation, a fact that could explain this difference. It seems reasonable to think that the number of radicals formed will increase with the concentration of potassium iodide as more radicals will be able to be scavenged by the dosimeter.

Another interesting pattern in relation to the concentration is that it becomes more important at concentrations higher than 0,7 mol/l, growing drastically the production of triiodide at 1 mol/l. The standard deviation at 10 °C is broadly high for all the tests, regardless of the concentration.

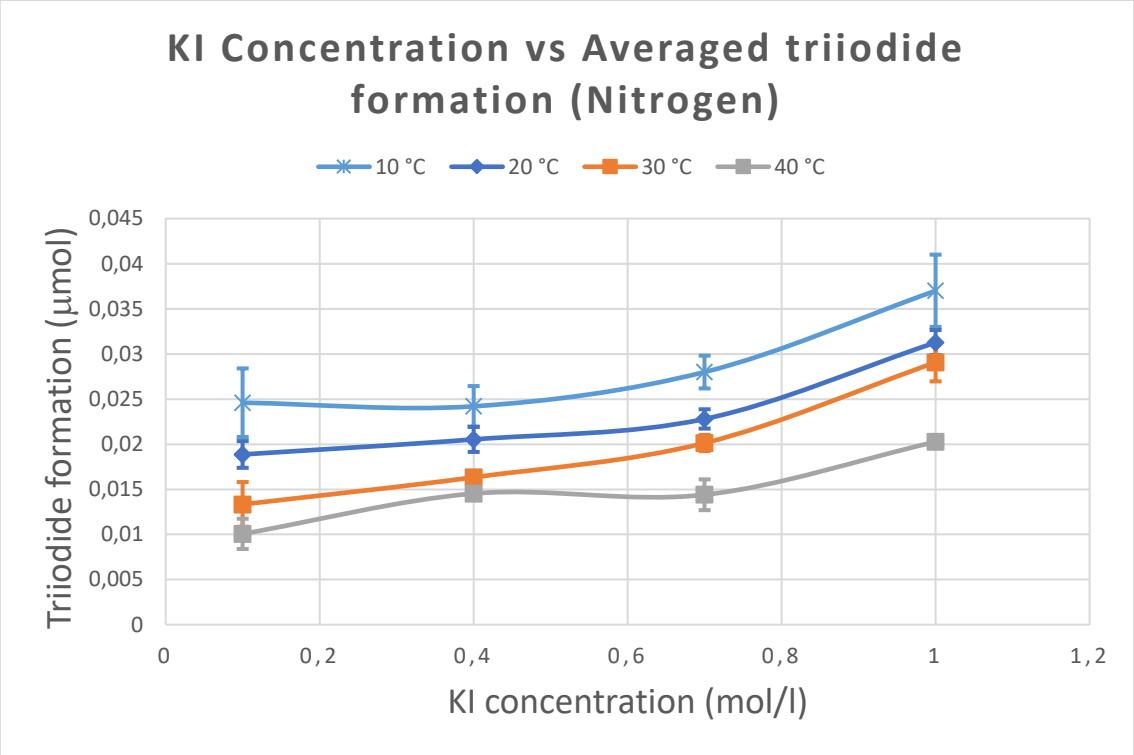

Figure 12: Effect of potassium iodide concentration on triiodide production for different initial solution temperatures, using nitrogen as a saturated gas and a frequency of 24 kHz. Water loop overpressurized (1,5 bar)

The effect of the initial solution temperature on triiodide formation is presented in Figure 13. The production of triiodide consistently decreases as the temperature increases, being the optimal temperature 10 °C. This considerable decline could be explained by the cushioning of the bubble collapse due to an increase of water vapor. A higher temperature also results in a lower polytropic index of the gas, which decreases sonochemical activity.

In general terms, the effect of the temperature can be modeled linearly. The production of triiodide in relation to temperature seems pretty similar with 0,1 M, 0,7 M and 1 M, especially for the last two concentrations. However, the results obtained for the 0,4 M are slightly different. While it is true that the main pattern is fulfilled (triiodide formation decreases with higher temperatures), the difference between 30 °C and 40 °C is not so significant.

These results are in good agreement with the findings of Merouani et al [59], who conducted a similar experiment but using a frequency of 300 kHz. In that work, the formation of triiodide also improved by increasing the concentration of potassium iodide. However, they attribute this effect to the variation of physical properties like surface tension or vapor pressure, which results in a more violent bubble collapse.

The optimum point was found at 10 °C, using a concentration of 1 M (0,037 µmol). In this case, it is important to consider the high dispersion of the samples.

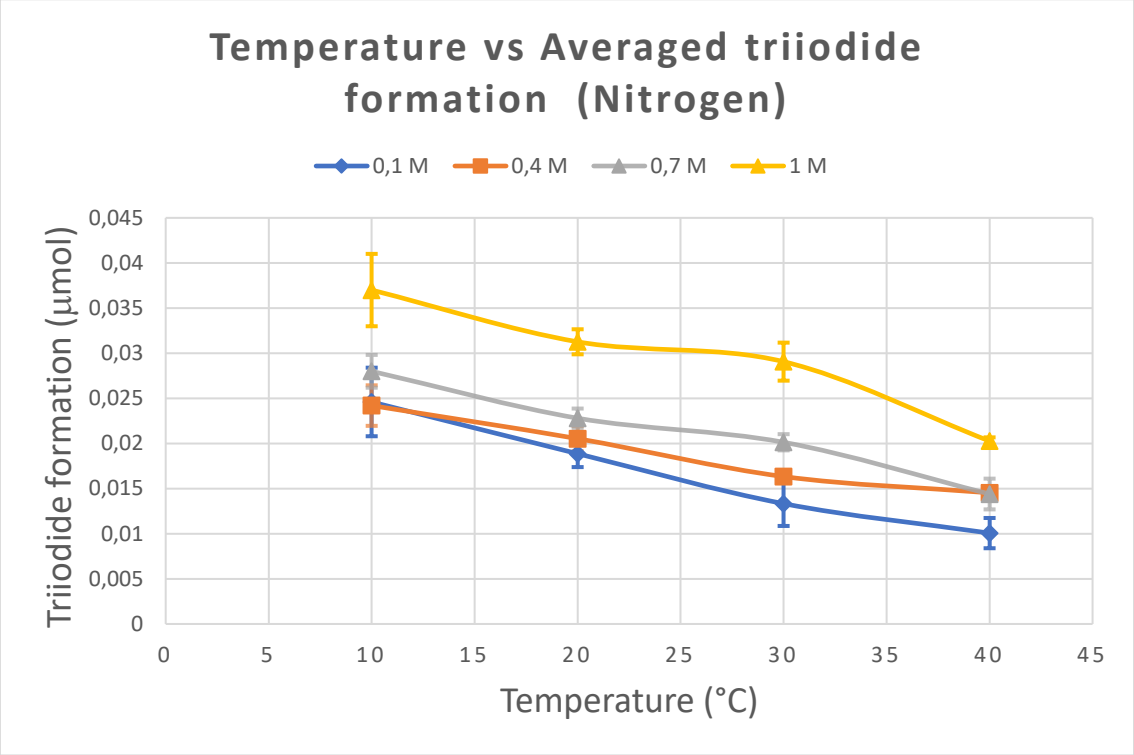

Figure 13: Effect of the initial solution temperature on triiodide production for different concentrations of potassium iodide, using nitrogen as a saturated gas and a frequency of 24 kHz. Water loop overpressurized (1,5 bar)

4.1.2 Argon

The fact of using argon instead of nitrogen results in a much higher triiodide yields for every temperature and concentration (Figure 14 and Figure 15), approximately by a factor of 3. It is also remarkable the fact that the optimum temperature for most of the concentrations is not the lowest one as with nitrogen but 20 °C. With 0,1 M concentration, the maximum was found at 30 °C. The effect of the concentration is more significant with argon, reaching a plateau at 1 mol/l.

While the behavior of the concentration can be modeled linearly and with better coefficient of determination than the results obtained with nitrogen, the effect of temperature cannot. The behavior of temperature is consistent with the computer simulation carried out by Merouani et al [35] for argon at lower frequencies. Another interesting fact of using argon as a saturated gas is that the temperature plays a minor role in the triiodide yields or, at least, its relevance is far less than the relevance when using nitrogen.

Regarding the dispersion of the samples, the standard deviation is generally good and, most importantly, it does not justify the change of the optimal temperature. Namely, the optimum point was found at 20 °C, using a concentration of 1 M (0,1306 µmol)

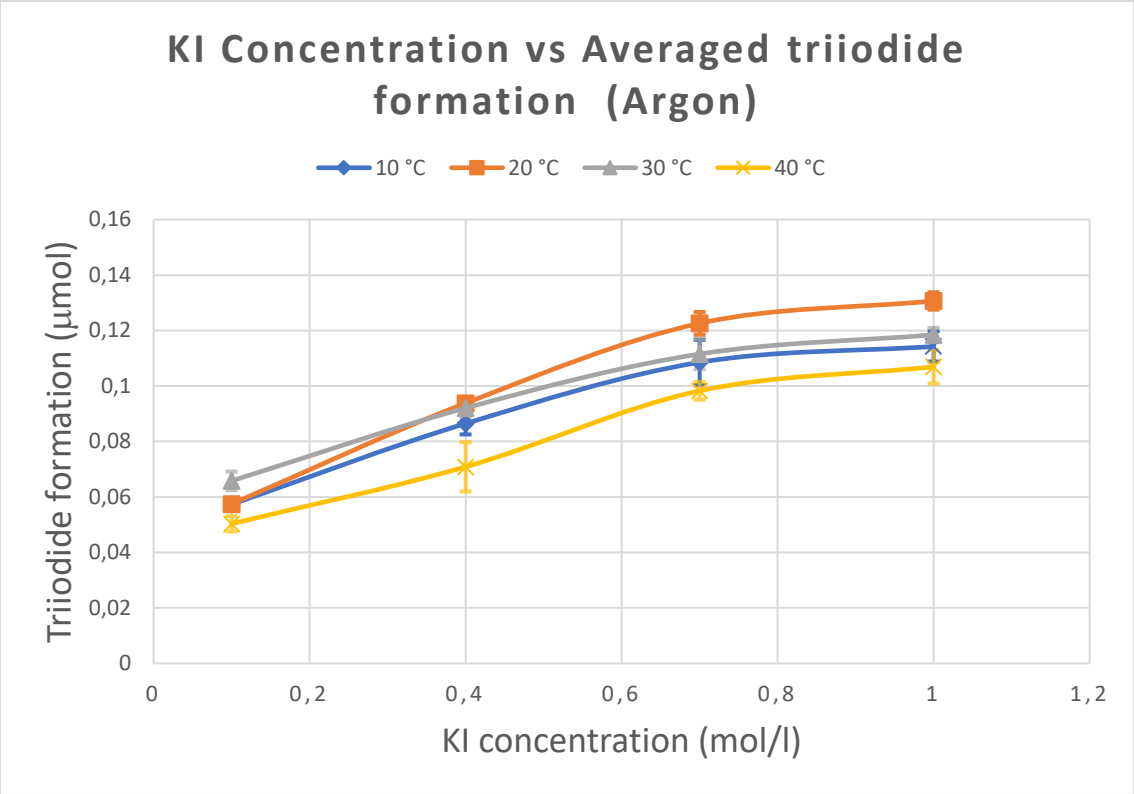

Figure 14: Effect of potassium iodide concentration on triiodide production for different initial solution temperatures, using argon as a saturated gas and a frequency of 24 kHz. Water loop overpressurized (1,5 bar)

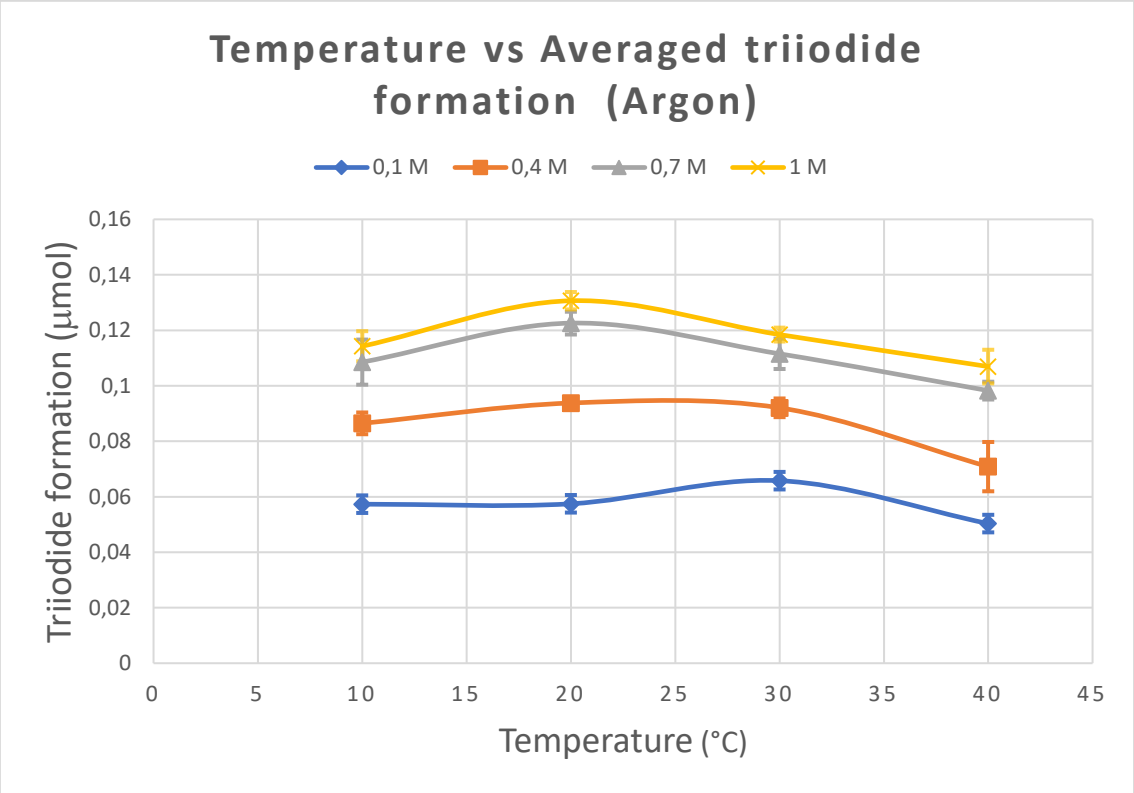

Figure 15: Effect of the initial solution temperature on triiodide production for different concentrations of potassium iodide, using argon as a saturated gas and a frequency of 24 kHz. Water loop overpressurized (1,5 bar)

4.1.3 Air

Air was the last gas to be tested with the Weissler dosimetry (Figure 16 and Figure 17). The effect of potassium iodide concentration on triiodide formation happened to be similar to the results obtained with other gases, however, a different behavior was seen for lower and higher temperatures. While with 10 °C and 20 °C the concentration has a strong impact on triiodide yields, with 30 °C and 40 °C the effects are less noticeable. It is also important to remark that at 10 °C, 20 °C and 40 °C the curves present similar slopes at higher concentrations, reaching a plateau at 1 mol/ l. For 20 °C it is slightly different, and a possible explanation of this difference is the high standard deviation obtained at 20 °C/ 0,7 mol/l (0,010123).

Regarding triiodide formation, air is the dissolved gas with the better performance of the three gases, being slightly higher than argon. The effect of the initial solution temperature and potassium iodide concentration strongly affects the sonochemical activity. An increase in the solution temperature results in a decrease of radical production. However, as temperature increases the impact on radical formation also decreases. This fact is particularly relevant after 30 °C, where the effect of temperature becomes almost negligible, reaching a plateau at 40 °C.

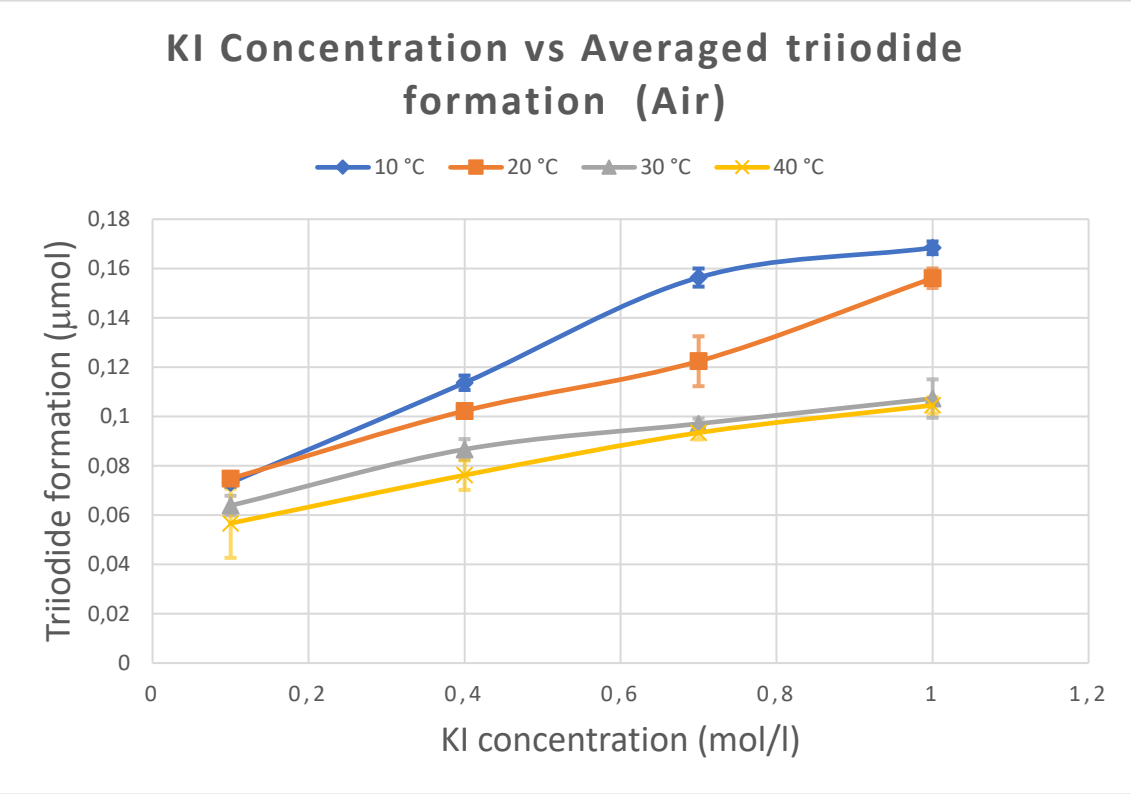

Figure 16: Effect of potassium iodide concentration on triiodide production for different initial solution temperatures, using air as a saturated gas. and a frequency of 24 kHz. Water loop overpressurized (1,5 bar)

Regarding the effect of temperature when a concentration of 0,1 mol/l is being used, it is possible to observe that, once again, the maximum is different from the other concentrations. Indeed, when argon was tested, the optimum temperature differed from the other concentrations. It is then legitimate to question the appropriateness of using concentrations of 0,1 M as a reliable and standardized test.

The production of triiodide reached a peak at 10 °C and 1 M (0,1684 µmol). This maximum value resulted to be the highest in regard to this dosimetry method.

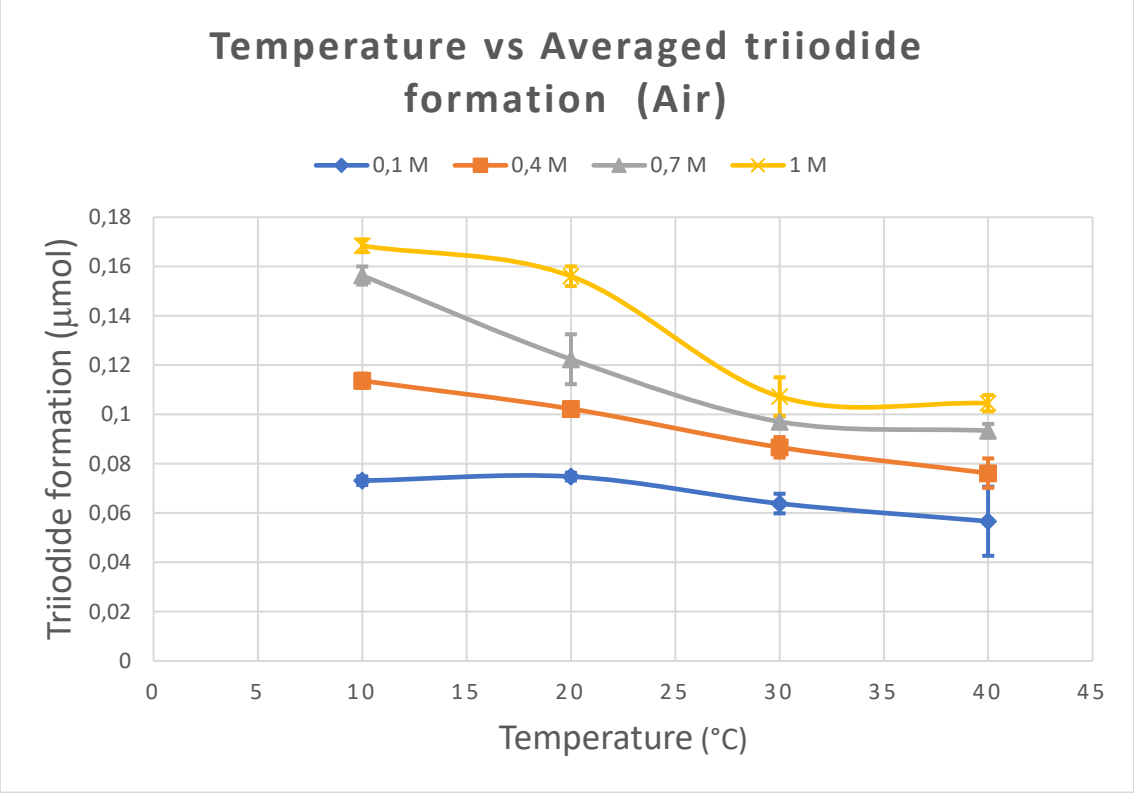

Figure 17: Effect of the initial solution temperature on triiodide production for different concentrations of potassium iodide, using air as a saturated gas and a frequency of 24 kHz. Water loop overpressurized (1,5 bar)

4.1.4 Effect of the water loop overpressure in sonochemical activity

Once the optimal configuration was found, it was considered convenient to test the effect of the water loop overpressure (Figure 18). Four different values of gauge pressure were tested, finding a negligible absorbance of 0,049 at 0 bar, an absorbance of 0,523 for 0,5 bar, a 0,845 absorbance for 1 bar and a 0,973 absorbance for the nominal overpressure at 1,5 bar. The results are presented in terms of absorbance at 350 nm, in other words, Beer-Lambert law has not been applied, but it is not necessary to do that to analyze the effect of overpressure on free radical formation.

A strong correlation can be observed between the overpressure and the sonochemical activity, being possible to fit a polynomial curve to this set of points. It becomes clear that overpressure plays a critical role in the results, specially between 0 and 1 bar.

As it has been stated above, the pressurization of the water loop reduces drastically the acoustic cavitation produced in the recirculated water, thus reaching more energy to the reactor cell.

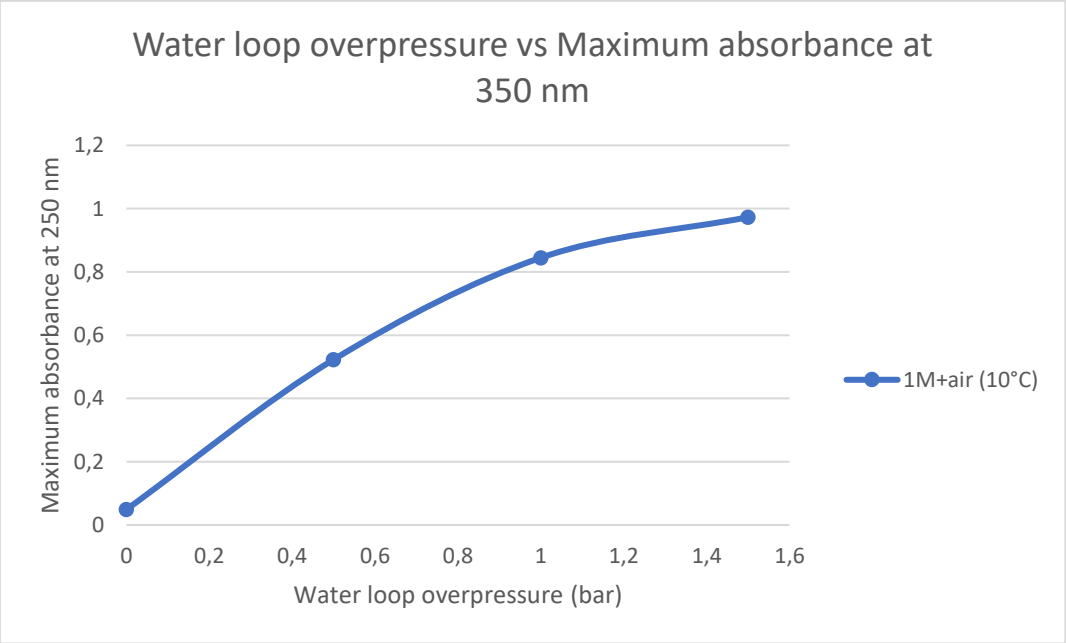

Figure 18: Impact of water loop overpressure in sonochemical activity at a frequency of 24 kHz

4.2 Fricke dosimetry

The Fricke dosimetry tests were conducted using argon and air as the production of triiodide and with it OH radical formation, resulted to be higher for these two gases. All the numerical data is also included in Appendix C.

The results obtained by means of this dosimetry method are more or less in accordance with the results found applying the potassium iodide dosimetry. However, these results should be treated with caution since the standard deviation is exceedingly high (especially for argon), as it can be noted in Figure 19. This wide dispersion cannot be explained because of the spectrophotometer used, inter alia, because Spectronic Helios Gamma spectrophotometer is more accurate that Genesys 30. Furthermore, some samples were analyzed with it during the Weissler dosimetry experiments, achieving good standard deviation values.

In principle, the effect of temperature on sonochemical activity seems to be more relevant with this dosimetry method than with the Weissler dosimeter, especially for argon. An important fact behind these results is that the optimal temperature for argon changes from 20 °C to 30 °C. Although it may be controversial to claim that 30 °C is the optimum temperature, as the dispersion is extremely high for these two temperatures, it is important to remark that, as was the case with the Weissler dosimetry results, the optimum temperature is not the lower, confirming the existence of a pattern.

Regarding the effect of temperature using air as a dissolved gas, it is similar to the results obtained before: the higher the temperature, the less radicals formed. However, unlike the Weissler dosimetry results, the effects of temperature are more noticeable beyond 30 °C, which is exactly the opposite behavior.

The optimum points are; 30°C for argon (0,3876 µmol of ferric ion),being the maximum value obtained in the Fricke dosimeter tests; and 10 °C for air (0,3717 µmol of ferric ion), which matches with the optimum point of air using the Weissler dosimetry.

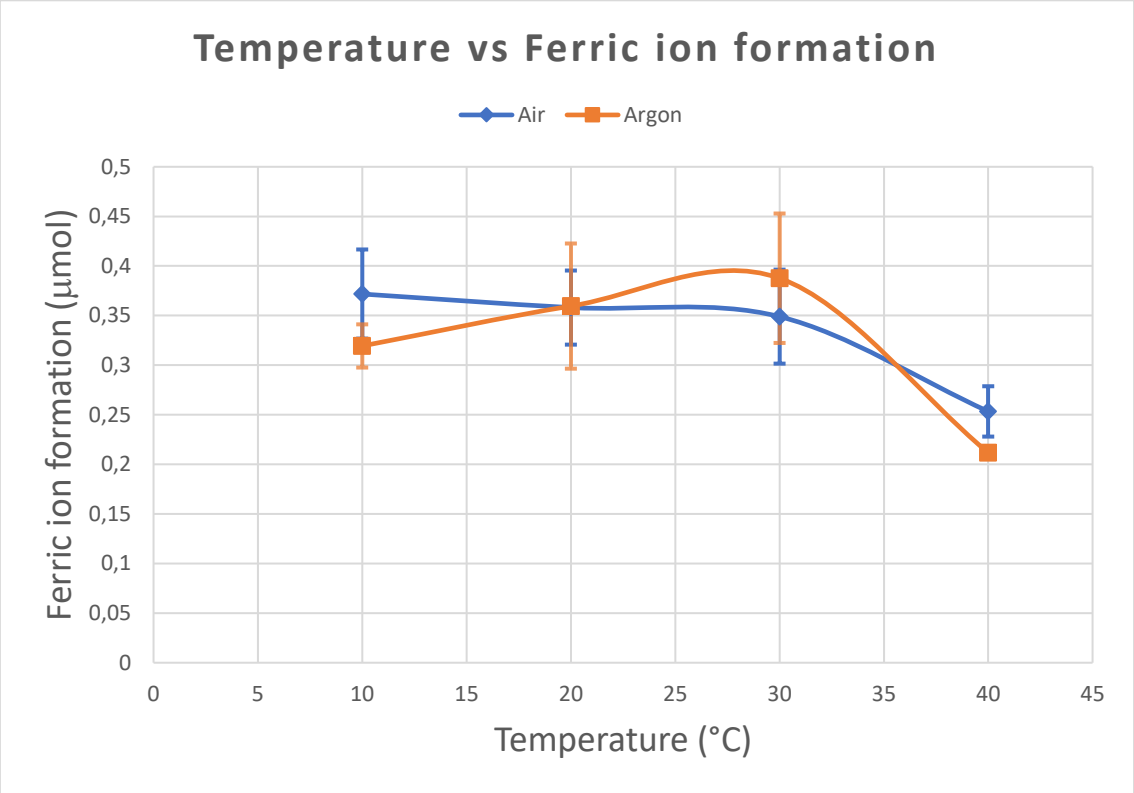

Figure 19: Effect of the initial solution temperature on ferric ion production for a standard concentration in the Fricke dosimetry ($(NH_4)_2Fe(SO_4)_2 \bullet 6H_2O$ (0,001 mol/l), H_2SO_4 (0,4 mol/l) and $NaCl$ (0,001 mol/l)), using air and argon as a saturated gases and a frequency of 24 kHz. Water loop overpressurized (1,5 bar)

4.3 Additional remarks and limitations of this work

The use of two different dosimetry methods seems convenient as there are many parameters involved in the formation of free radicals that could be ignored since a chemical compound is being used as an indirect indicator, and this indicator could be influenced by other factors. The results obtained for both dosimetry methods certainly give a clearer and more complete picture of the effect of these different parameters. While some of the patterns found in the Weissler dosimetry experiments are clearly confirmed such as the evolution of sonochemical activity with the temperature using air, other features are discovered: higher yields than expected when using argon as a saturated gas have been obtained, for instance.

Although air was the dissolved gas which produced the higher amount of triiodide, the yields of triiodide at 30 °C were higher for argon (Figure 20), which is also consistent with the results obtained with the Fricke dosimetry tests. Nevertheless, which is particularly interesting is that in these last tests, the maximum global production is achieved using argon and not air (Figure 19).

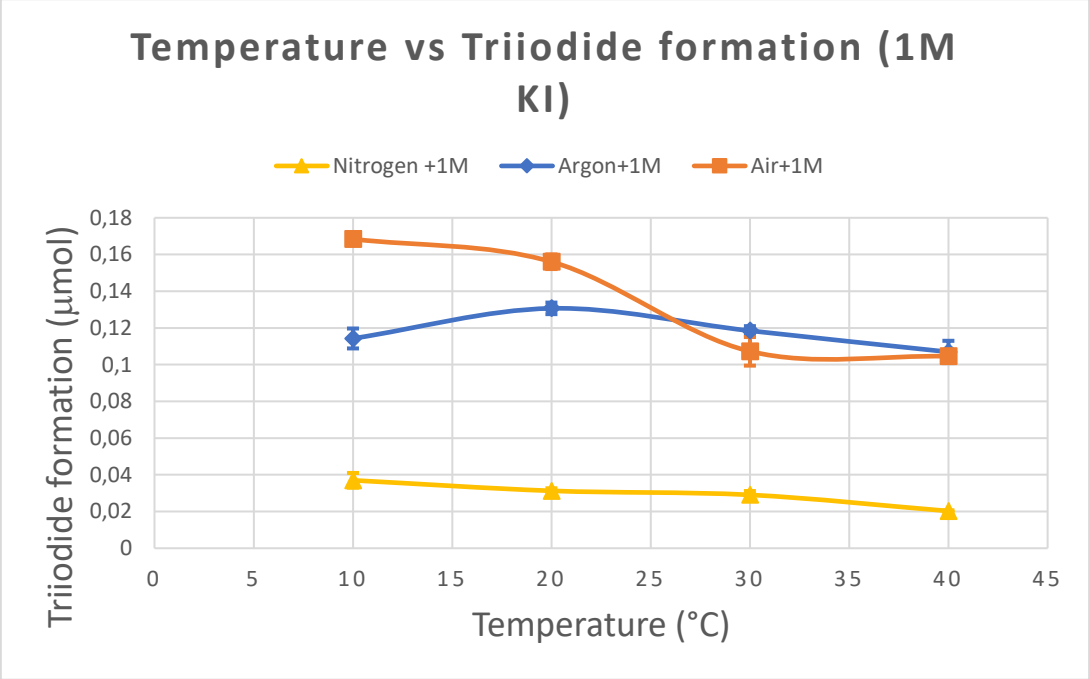

Figure 20: Effect of the initial solution temperature on triiodide production using air, nitrogen and argon as saturated gases with a concentration of 1M KI and a frequency of 24 kHz. Water loop overpressurized (1,5 bar)

The dispersion obtained in the Fricke dosimetry tests is certainly strange. An interesting experiment where Weissler and Fricke dosimetry methods were tested at different frequencies (from 19,5 kHz to 1,2 MHz) was conducted by Koda et al [42]. The results of this work did not show a higher dispersion for the Fricke dosimetry tests, furthermore, the experiments conducted by means of the Weissler dosimetry presented a slightly higher dispersion.

As it has been mentioned above, an important parameter that affects sonochemical activity is the bubble collapse temperature, which is strongly related to the polytropic ratio and the heat conductivity. That way, a high polytropic ratio and a low heat conductivity increase the bubble collapse temperature [47]. The viscosity also affects the radical yields as a lower Viscosity decreases the cavitation threshold [38]. All these parameters are presented in Table 3 [60], [61] for the gases used in this work.

Table 3: Properties of the different gases under consideration for this work [60], [61]

Gas	Viscosity ($\mu Pa \cdot s$)	Thermal conductivity ($mW/m \cdot K$)	Polytropic index
Air	18,523	26,3529	1,4
Argon	22,7241	17,8042	1,661
Nitrogen	17,8771	25,9361	1,401

A higher thermal conductivity of nitrogen coupled to its lower polytropic index could offer a good explanation in regard to the poor performance of nitrogen on the production of reactive species. Furthermore, in spite of the fact that argon has a higher viscosity, it has the best and most important properties to enhance bubble collapse temperature and thus radical formation.

In contrast, air is a gas that is supposed to perform badly but achieves the best results in the Weissler dosimetry tests, nonetheless. This enhancement is believed to be related to chemical effects and not with physical properties [47]. Several authors have tested the effect on sonochemical activity of both argon and air, concluding that frequency plays a major role, among other things [35], [38], [47], [62]–[64].

The fact that the optimal temperature is not the lowest one when argon is used could be explained by the increase of water vapor trapped in the bubbles (more radicals could be formed) or a decrease in the viscosity, which, decreases the cavitation threshold. As it has been mentioned above, this increase of water vapor could also cushion the collapse of the bubble, reducing free radical yields. Furthermore, the polytropic index and the gas solubility decrease with temperature. Therefore, it is difficult to analyze the effects of the solution temperature.

Iida et al [64] compared the sonochemical activity of argon, air and nitrogen by means of the Fricke dosimeter at 130 kHz , obtaining the best results for argon and the poorer performance for nitrogen, which could be in accordance with the results obtained in this work. The effect of frequency on OH radical formation is certainly important, and it has a significant impact on the obtention of reactive species; however, it has not been considered for this Master's Thesis.

There are other effects besides frequency that could be important to analyze. For example, it has been reported that the pH has an important impact on triiodide formation in the Weissler dosimetry [59], [64]. The ultrasonic intensity and other parameters such as liquid height or the type of transducer used could be important for OH radical obtention.

5 Conclusion

The influence of several parameters on hydroxyl radical formation by ultrasonic irradiation was evaluated in this Master's Thesis, using Weissler and Fricke dosimetry methods as characterization tools. The tests were conducted at a simple 24 kHz frequency, using a double wall Besançon microsonoreactor, being the water loop pressurized at 1,5 bar. Additionally, this overpressure was also studied in order to determine its effect on radical formation, resulting to be a critical parameter. The use of two different dosimetry methods proved to be important as a better reliability was achieved, finding patterns that were not seen with only one dosimetry method.

The effect of potassium iodide concentration affected the production of triiodide, obtaining higher yields with higher concentrations. Hence, the highest levels of triiodide concentration were obtained at 1 mol/l of KI for every saturated gas. The results also show that using a single concentration of 0,1 mol/l of KI as a standardized test may be insufficient, as the optimum temperature changed for both argon and air with this concentration.

Regarding the solution temperature, it was found that the higher the temperature the lower the obtention of OH radicals for argon and air, obtaining the best results at 10 °C. However, in the case of Argon, the optimum temperature resulted to be between 20 °C and 30 °C. Many parameters are influenced by the solution temperature, being difficult to extract accurate conclusions.

The effect of the dissolved gas on OH formation was very significant. The gas with worst performance was nitrogen by far. Nevertheless, the identification of the best gas is questionable, as air had the best performance during the Weissler dosimetry tests and argon obtained better results during the Fricke dosimetry experiments. It is important to add that the dispersion obtained with the Fricke dosimeter method was very high, especially for argon. This issue, along with the fact that air and argon obtained similar maximum production rates during the Fricke dosimetry, leads to the conclusion that air is probably the better saturated gas with these conditions.

The experiments were the water loop overpressure was varied, showed a very important enhancement on OH obtention, especially at lower pressures. Beyond 1 bar the sonochemical activity kept growing but at lower rates.

It has been proven that the effects of applying power ultrasound into an aqueous solution are complex and difficult to analyze as these effects depend on many factors. In order to have a more complete view, it would be convenient to analyze the effect of other parameters such as pH or ultrasonic intensity. Further research is still needed to understand the mechanisms involved in the sonochemical production of hydrogen.

Bibliography

[1] R. M. Cuéllar-Franca and A. Azapagic, "Carbon capture, storage and utilisation technologies: A critical analysis and comparison of their life cycle environmental impacts," *J. CO2 Util.*, vol. 9, pp. 82–102, 2015.

[2] M. E. Mann, R. S. Bradley, and M. K. Hughes, "Northern hemisphere temperatures during the past millennium: Inferences, uncertainties, and limitations," *Geophys. Res. Lett.*, vol. 26, no. 6, pp. 759–762, 1999.

[3] S. Levitus *et al.*, "World ocean heat content and thermosteric sea level change (0–2000 m), 1955–2010," *Geophys. Res. Lett.*, vol. 39, pp. 1–5, 2012.

[4] C. D. Keeling, J. A. Adams Jr., C. A. Ekdahl Jr., and P. R. Guenther, "Atmospheric carbon dioxide variations at the South Pole," *Tellus*, vol. 28, no. 6, pp. 552–564, 1976.

[5] , Allen *et al.*, *Climate Change 2014: Synthesis Report*. 2014.

[6] BP, "BP Statistical Review of World Energy 2018," 2018.

[7] M. H. Islam, O. S. Burheim, and B. G. Pollet, "Sonochemical and sonoelectrochemical production of hydrogen," *Ultrason. Sonochem.*, vol. 51, pp. 533–555, Mar. 2019.

[8] R. G. Compton, J. C. Eklund, and F. Marken, "Sonoelectrochemical Processes: A Review," *Electroanalysis*, vol. 9, pp. 509–522, 1997.

[9] T. A. Mamvura, S. E. Iyuke, and A. E. Paterson, "Energy changes during use of high-power ultrasound on food grade surfaces," *South African J. Chem. Eng.*, vol. 25, pp. 62–73, 2018.

[10] M. Legay, N. Gondrexon, S. Le Person, P. Boldo, and A. Bontemps, "Enhancement of Heat Transfer by Ultrasound: Review and Recent Advances," *Int. J. Chem. Eng.*, vol. 2011, 2011.

[11] B. Thokchom, A. B. Pandit, P. Qiu, B. Park, J. Choi, and J. Khim, "A review on sonoelectrochemical technology as an upcoming alternative for pollutant degradation," *Ultrason. Sonochem.*, vol. 27, pp. 210–234, 2015.

[12] J. González-García, M. D. Esclapez, P. Bonete, Y. V. Hernández, L. G. Garretón, and V. Sáez, "Current topics on sonoelectrochemistry," *Ultrasonics*, vol. 50, no. 2, pp. 318–322, 2010.

[13] N. MORIGUCHI, "The Influence of Supersonic Waves on Chemical Phenomena. III," *Nippon KAGAKU KAISHI*, vol. 55, no. 8, pp. 749–750, 1934.

[14] D. Symes, "Sonoelectrochemical (20 Khz) Production of Hydrogen from Aqueous Solutions," 2011.

[15] D. J. Walton, L. D. Burke, and M. M. Murphy, "Sonoelectrochemistry: Chlorine, hydrogen and oxygen evolution at platinised platinum," *Electrochim. Acta*, vol. 41, no. 17, pp. 2747–2751, 1996.

[16] C. Budischak, C. Honsberg, and R. L. Opila, “Electroanalytic effects of ultrasound on a hydrogen evolution reaction in KOH,” in *2008 33rd IEEE Photovoltaic Specialists Conference*, 2008, pp. 1–3.

[17] C. Hagan and L. A. Coury, “Comparison of hydrodynamic voltammetry implemented by sonication to a rotating disk electrode,” *Anal. Chem. - ANAL CHEM*, vol. 66, 1994.

[18] A. Durant, H. François, J. Reisse, and A. Kirsch-DeMesmaeker, “Sonoelectrochemistry: The effects of ultrasound on organic electrochemical reduction,” *Electrochim. Acta*, vol. 41, no. 2, pp. 277–284, 1996.

[19] Y. Fang, T. Yamamoto, and S. Komarov, “Cavitation and acoustic streaming generated by different sonotrode tips,” *Ultrason. Sonochem.*, vol. 48, pp. 79–87, 2018.

[20] J. Klima, “Application of ultrasound in electrochemistry. An overview of mechanisms and design of experimental arrangement,” *Ultrasonics*, vol. 51, no. 2, pp. 202–209, 2011.

[21] R. F. Contamine, A. M. Wilhelm, J. Berlan, and H. Delmas, “Power measurement in sonochemistry,” *Ultrason. Sonochem.*, vol. 2, no. 1, pp. S43–S47, 1995.

[22] M. Takahashi, K. Chiba, and P. Li, “Free-radical generation from collapsing microbubbles in the absence of a dynamic stimulus,” *The Journal of Physical Chemistry B*, vol. 111. 2007.

[23] B. Pollet and O. J. Curnick, “Power Ultrasound in Electrochemistry: From Versatile Laboratory Tool to Engineering Solution,” in *Power Ultrasound in Electrochemistry: From Versatile Laboratory Tool to Engineering Solution*, 2012, pp. 1–20.

[24] M. Kohno, T. Mokudai, T. Ozawa, and Y. Niwano, “Free radical formation from sonolysis of water in the presence of different gases,” *J. Clin. Biochem. Nutr.*, vol. 49, pp. 96–101, 2011.

[25] K. Takeda, K. Fujisawa, H. Nojima, R. Kato, R. Ueki, and H. Sakugawa, “Hydroxyl radical generation with a high power ultraviolet light emitting diode (UV-LED) and application for determination of hydroxyl radical reaction rate constants,” *J. Photochem. Photobiol. A Chem.*, vol. 340, pp. 8–14, 2017.

[26] J. Klíma and C. Bernard, “Sonoassisted electrooxidative polymerisation of salicylic acid: role of acoustic streaming and microjetting,” *J. Electroanal. Chem.*, vol. 462, no. 2, pp. 181–186, 1999.

[27] F. Marken, S. Kumbhat, G. H. W. Sanders, and R. G. Compton, “Voltammetry in the presence of ultrasound: surface and solution processes in the sonovoltammetric reduction of nitrobenzene at glassy carbon and gold electrodes,” *J. Electroanal. Chem.*, vol. 414, no. 2, pp. 95–105, 1996.

[28] S. Afreen, K. Muthoosamy, and S. Manickam, “Sono-nano chemistry: A new era of synthesising polyhydroxylated carbon nanomaterials with hydroxyl groups and their industrial aspects,” *Ultrason. Sonochem.*, vol. 51, pp. 451–461, 2019.

[29] T. Mason and , J.P.Lorimer, *Applied Sonochemistry: The Uses of Power Ultrasound in Chemistry and Processing*. 2002.

[30] A. Mayyas and M. Mann, “Emerging Manufacturing Technologies for Fuel Cells and Electrolyzers,” *Procedia Manuf.*, vol. 33, pp. 508–515, 2019.

[31] M. Ashokkumar, “The characterization of acoustic cavitation bubbles – An overview,” *Ultrason. Sonochem.*, vol. 18, no. 4, pp. 864–872, 2011.

[32] S. Merouani and O. Hamdaoui, “The size of active bubbles for the production of hydrogen in sonochemical reaction field,” *Ultrason. Sonochem.*, vol. 32, pp. 320–327, 2016.

[33] P. Riesz, D. Berdahl, and C. L Christman, “Free Radical Generation by Ultrasound in Aqueous and Nonaqueous Solutions,” *Environ. Health Perspect.*, vol. 64, pp. 233–252, 1986.

[34] S. Merouani, O. Hamdaoui, Y. Rezgui, and M. Guemini, “Mechanism of the sonochemical production of hydrogen,” *Int. J. Hydrogen Energy*, vol. 40, no. 11, pp. 4056–4064, 2015.

[35] S. Merouani, O. Hamdaoui, Y. Rezgui, and M. Guemini, “Computational engineering study of hydrogen production via ultrasonic cavitation in water,” *Int. J. Hydrogen Energy*, vol. 41, no. 2, pp. 832–844, 2016.

[36] K. Yasui, “Chapter 3 - Dynamics of Acoustic Bubbles,” in *Sonochemistry and the Acoustic Bubble*, F. Grieser, P.-K. Choi, N. Enomoto, H. Harada, K. Okitsu, and K. Yasui, Eds. Amsterdam: Elsevier, 2015, pp. 41–83.

[37] S. Merouani, O. Hamdaoui, R. Yacine, and M. Guemini, “Optimum Bubble Temperature for the Production of Hydroxyl Radical in Acoustic Cavitation – Frequency Dependence,” *Acta Acust. united with Acust.*, vol. 101, 2015.

[38] R. J. Wood, J. Lee, and M. J. Bussemaker, “A parametric review of sonochemistry: Control and augmentation of sonochemical activity in aqueous solutions,” *Ultrason. Sonochem.*, vol. 38, pp. 351–370, 2017.

[39] K. Yasui, “Influence of ultrasonic frequency on multibubble sonoluminescence,” *J. Acoust. Soc. Am.*, vol. 112, no. 4, pp. 1405–1413, 2002.

[40] T. Leong, M. Ashokkumar, and S. Kentish, “THE FUNDAMENTALS OF POWER ULTRASOUND - A REVIEW,” vol. 39, no. ACOUSTICS AUSTRALIA, pp. 54–63, Jan. 2017.

[41] K. Yasui, T. Tuziuti, J. Lee, T. Kozuka, A. Towata, and Y. Iida, “The range of ambient radius for an active bubble in sonoluminescence and sonochemical reactions,” *J. Chem. Phys.*, vol. 128, p. 184705, 2008.

[42] S. Koda, T. Kimura, T. Kondo, and H. Mitome, “A standard method to calibrate sonochemical efficiency of an individual reaction system,” *Ultrason. Sonochem.*, vol. 10, no. 3, pp. 149–156, 2003.

[43] A. Brotchie, F. Grieser, and M. Ashokkumar, “Effect of Power and Frequency on Bubble-Size Distributions in Acoustic Cavitation,” *Phys. Rev. Lett.*, vol. 102, p.

84302, 2009.

[44] S. Hatanaka, H. Mitome, K. Yasui, and S. Hayashi, “Multibubble sonoluminescence enhancement by fluid flow,” *Ultrasonics*, vol. 44, pp. e435–e438, 2006.

[45] K. Yasui, T. Tuziuti, and Y. Iida, “Optimum bubble temperature for the sonochemical production of oxidants,” *Ultrasonics*, vol. 42, no. 1, pp. 579–584, 2004.

[46] S. Merouani, O. Hamdaoui, Y. Rezgui, and M. Guemini, “Theoretical estimation of the temperature and pressure within collapsing acoustical bubbles,” *Ultrason. Sonochem.*, vol. 21, no. 1, pp. 53–59, 2014.

[47] J. Rooze, E. V Rebrov, J. C. Schouten, and J. T. F. Keurentjes, “Dissolved gas and ultrasonic cavitation – A review,” *Ultrason. Sonochem.*, vol. 20, no. 1, pp. 1–11, 2013.

[48] E. Dalodière, M. Virot, P. Moisy, and S. I. Nikitenko, “Effect of ultrasonic frequency on H2O2 sonochemical formation rate in aqueous nitric acid solutions in the presence of oxygen,” *Ultrason. Sonochem.*, vol. 29, pp. 198–204, 2016.

[49] A. Ebrahiminia, M. Mokhtari-Dizaji, and T. Toliyat, “Correlation between iodide dosimetry and terephthalic acid dosimetry to evaluate the reactive radical production due to the acoustic cavitation activity,” *Ultrason. Sonochem.*, vol. 20, no. 1, pp. 366–372, 2013.

[50] M. Hodnett, “8 - Measurement techniques in power ultrasonics,” in *Power Ultrasonics*, J. A. Gallego-Juárez and K. F. Graff, Eds. Oxford: Woodhead Publishing, 2015, pp. 195–218.

[51] T. Mason, *Advances in Sonochemistry, Volume 5*. 1999.

[52] L. Mizina and S. Kulyukhin, “New Composite Materials for Decreasing of Radioactive Molecular Iodine in the Water Coolant in Working and New Developed NPPs,” in *Metal, Ceramic and Polymeric Composites for Various Uses*, J. Cuppoletti, Ed. Rijeka: IntechOpen, 2011.

[53] C. E. deAlmeida *et al.*, “A feasibility study of Fricke dosimetry as an absorbed dose to water standard for 192Ir HDR sources,” *PLoS One*, vol. 9, no. 12, pp. e115155–e115155, Dec. 2014.

[54] R. W. Matthews, “Aqueous chemical dosimetry,” *Int. J. Appl. Radiat. Isot.*, vol. 33, no. 11, pp. 1159–1170, 1982.

[55] S. de La Rochebrochard d’Auzay, J.-F. Blais, and E. Naffrechoux, “Comparison of characterization methods in high frequency sonochemical reactors of differing configurations,” *Ultrason. Sonochem.*, vol. 17, no. 3, pp. 547–554, 2010.

[56] L. Villeneuve, L. Alberti, J.-P. Steghens, J.-M. Lancelin, and J.-L. Mestas, “Assay of hydroxyl radicals generated by focused ultrasound,” *Ultrason. Sonochem.*, vol. 16, no. 3, pp. 339–344, 2009.

[57] T. J. Mason, J. P. Lorimer, D. M. Bates, and Y. Zhao, “Dosimetry in

sonochemistry: the use of aqueous terephthalate ion as a fluorescence monitor," *Ultrason. Sonochem.*, vol. 1, no. 2, pp. S91–S95, 1994.

[58] S. Kanazawa, T. Furuki, T. Nakaji, S. Akamine, and R. Ichiki, "Application of chemical dosimetry to hydroxyl radical measurement during underwater discharge," *J. Phys. Conf. Ser.*, vol. 418, p. 12102, Mar. 2013.

[59] S. Merouani, O. Hamdaoui, F. Saoudi, and M. Chiha, "Influence of experimental parameters on sonochemistry dosimetries: KI oxidation, Fricke reaction and H2O2 production," *J. Hazard. Mater.*, vol. 178, no. 1, pp. 1007–1014, 2010.

[60] A. A. Allan D. Kraus, James R. Welty, *Introduction to Thermal and Fluids Engineering*. 2011.

[61] E. W. Lemmon and R. T. Jacobsen, "Viscosity and Thermal Conductivity Equations for Nitrogen, Oxygen, Argon, and Air," *Int. J. Thermophys.*, vol. 25, pp. 21–69, 2004.

[62] M. H. Entezari and P. Kruus, "Effect of frequency on sonochemical reactions. I: Oxidation of iodide," *Ultrason. Sonochem.*, vol. 1, no. 2, pp. S75–S79, 1994.

[63] E. L. Mead, R. G. Sutherland, and R. E. Verrall, "The effect of ultrasound on water in the presence of dissolved gases," *Can. J. Chem.*, vol. 54, pp. 1114–1120, 2011.

[64] Y. Iida, K. Yasui, T. Tuziuti, and M. Sivakumar, "Sonochemistry and its dosimetry," *Microchem. J.*, vol. 80, no. 2, pp. 159–164, 2005.

Appendix A Experimental plan

Table 4: Programmed tests for nitrogen by means of the Weissler dosimetry method

Nitrogen (Weissler Dosimetry)												
	Temperature											
Concentration	10 °C			20 °C			30 °C			40 °C		
0,1 M	Test 1	Test 2	Test 3	Test 4	Test 5	Test 6	Test 7	Test 8	Test 9	Test 10	Test 11	Test 12
0,4 M	Test 13	Test 14	Test 15	Test 16	Test 17	Test 18	Test 19	Test 20	Test 21	Test 22	Test 23	Test 24
0,7 M	Test 25	Test 26	Test 27	Test 28	Test 29	Test 30	Test 31	Test 32	Test 33	Test 34	Test 35	Test 36
1 M	Test 37	Test 38	Test 39	Test 40	Test 41	Test 42	Test 43	Test 44	Test 45	Test 46	Test 47	Test 48

Table 5: Programmed tests for argon by means of the Weissler dosimetry method

Argon (Weissler Dosimetry)												
	Temperature											
Concentration	10 °C			20 °C			30 °C			40 °C		
0,1 M	Test 49	Test 50	Test 51	Test 52	Test 53	Test 54	Test 55	Test 56	Test 57	Test 58	Test 59	Test 60
0,4 M	Test 61	Test 62	Test 63	Test 64	Test 65	Test 66	Test 67	Test 68	Test 69	Test 70	Test 71	Test 72
0,7 M	Test 73	Test 74	Test 75	Test 76	Test 77	Test 78	Test 79	Test 80	Test 81	Test 82	Test 83	Test 84
1 M	Test 85	Test 86	Test 87	Test 88	Test 89	Test 90	Test 91	Test 92	Test 93	Test 94	Test 95	Test 96

Table 6: Programmed tests for air by means of the Weissler dosimetry method

Air (Weissler Dosimetry)												
	Temperature											
Concentration	10 °C			20 °C			30 °C			40 °C		
0,1 M	Test 97	Test 98	Test 99	Test 100	Test 101	Test 102	Test 103	Test 104	Test 105	Test 106	Test 107	Test 108
0,4 M	Test 109	Test 110	Test 111	Test 112	Test 113	Test 114	Test 115	Test 116	Test 117	Test 118	Test 119	Test 120
0,7 M	Test 120	Test 121	Test 122	Test 123	Test 124	Test 125	Test 126	Test 127	Test 128	Test 129	Test 130	Test 131
1 M	Test 132	Test 133	Test 134	Test 135	Test 136	Test 137	Test 138	Test 139	Test 140	Test 141	Test 142	Test 143

Table 7: Programmed tests for the optimum gas in the Weissler dosimetry experiments by means of the Fricke dosimetry method

First Gas (Fricke Dosimetry)											
Temperature											
10 °C			20 °C			30 °C			40 °C		
Test 144	Test 145	Test 146	Test 147	Test 148	Test 149	Test 150	Test 151	Test 152	Test 153	Test 154	Test 155

Table 8: Programmed tests for the second best gas in the Weissler dosimetry experiments by means of the Fricke dosimetry method

Second Gas (Fricke Dosimetry)											
Temperature											
10 °C			20 °C			30 °C			40 °C		
Test 156	Test 156	Test 157	Test 158	Test 159	Test 160	Test 161	Test 162	Test 163	Test 164	Test 165	Test 166

Appendix B Gas saturation time tests

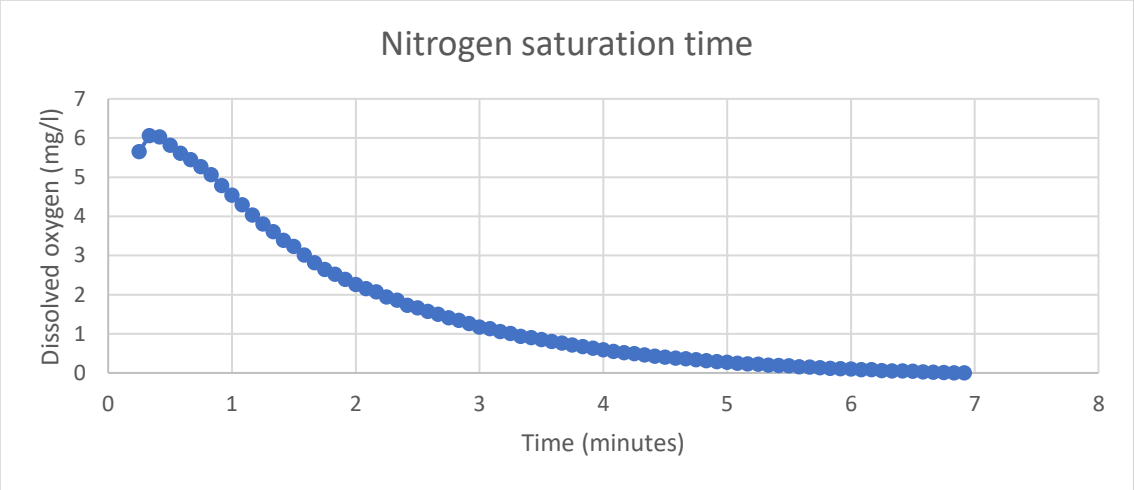

Figure 21: Dissolved oxygen evolution for nitrogen during the DO tests

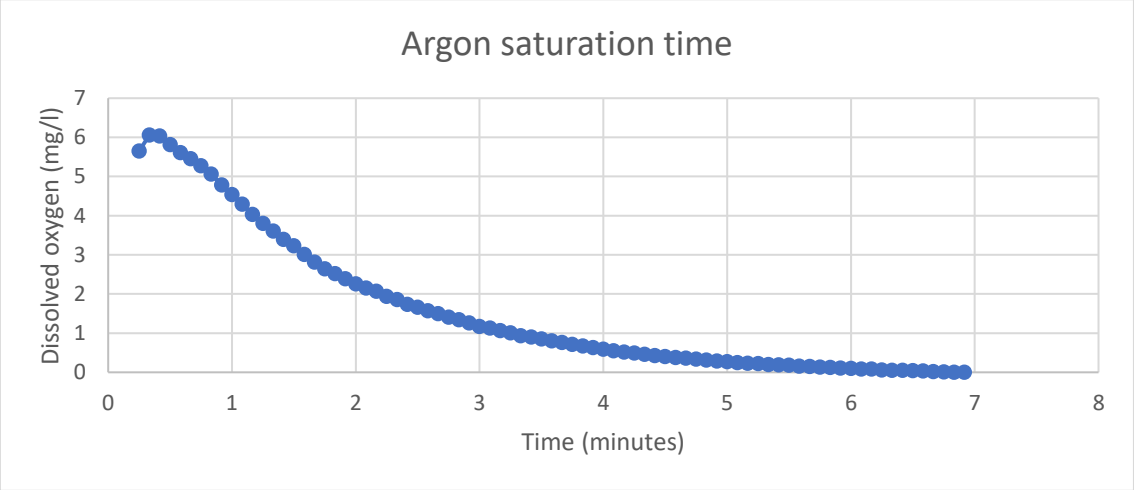

Figure 22: Dissolved oxygen evolution for argon during the DO tests

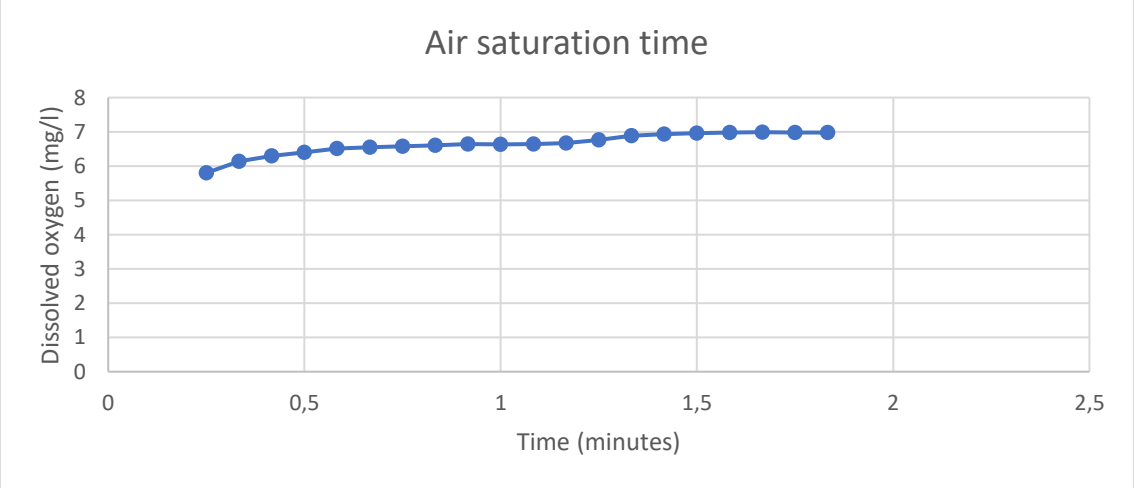

Figure 23: Dissolved oxygen evolution for air during the DO tests

Appendix C Results

a) Weissler dosimetry with nitrogen

Table 9: Triiodide production using nitrogen (µmol)

	Temperature											
Concentration	10 °C			20 °C			30 °C			40 °C		
0,1 M	0,0204	0,0238	0,0296	0,0196	0,0168	0,0202	0,0168	0,012	0,0112	0,0078	0,0106	0,0118
Standard deviation	0,003798245			0,001481741			0,002472965			0,001675974		
Average	0,0246			0,018866667			0,013333333			0,010066667		
0,4 M	0,0218	0,0236	0,0272	0,0212	0,0218	0,0186	0,0162	0,0158	0,017	0,0136	0,0148	0,0152
Standard deviation	0,002244994			0,001388844			0,000498888			0,000679869		
Average	0,0242			0,020533333			0,016333333			0,014533333		
0,7 M	0,0276	0,0304	0,026	0,024	0,023	0,0214	0,0196	0,0214	0,0194	0,012	0,0154	0,0158
Standard deviation	0,001818424			0,001070825			0,000899383			0,001704895		
Average	0,028			0,0228			0,020133333			0,0144		
1 M	0,0382	0,0412	0,0316	0,033	0,0312	0,0296	0,0262	0,0298	0,0312	0,0202	0,0208	0,0198
Standard deviation	0,004009988			0,001388844			0,002106076			0,000410961		
Average	0,037			0,031266667			0,029066667			0,020266667		

b) Weissler dosimetry with argon

Table 10: Triiodide production using argon (µmol)

	Temperature											
Concentration	10 °C			20 °C			30 °C			40 °C		
0,1 M	0,059	0,0542	0,0588	0,058	0,056	0,0584	0,0704	0,0646	0,0624	0,0528	0,0518	0,0464
Standard deviation	0,002217105			0,001049868			0,003374414			0,002811089		
Average	0,057333333			0,057466667			0,0658			0,050333333		
0,4 M	0,0834	0,092	0,084	0,0934	0,0942	0,0938	0,0874	0,0936	0,0952	0,0668	0,0626	0,0832
Standard deviation	0,003920317			0,000326599			0,00336386			0,008887944		
Average	0,086466667			0,0938			0,092066667			0,070866667		
0,7 M	0,102	0,1036	0,12	0,12	0,1284	0,1194	0,1048	0,1182	0,1116	0,0958	0,0962	0,1028
Standard deviation	0,008134426			0,004108528			0,00547073			0,003209707		
Average	0,108533333			0,1226			0,111533333			0,098266667		
1 M	0,1218	0,1118	0,1092	0,1272	0,1348	0,13	0,122	0,1168	0,1166	0,1004	0,1054	0,115
Standard deviation	0,005431595			0,003138294			0,002499778			0,006058236		
Average	0,114266667			0,130666667			0,118466667			0,106933333		

c) Weissler dosimetry with air

Table 11: Triiodide production using air (µmol)

	Temperature											
Concentration	10 °C			20 °C			30 °C			40 °C		
0,1 M	0,0718	0,0756	0,072	0,0756	0,0762	0,0726	0,0584	0,0654	0,0678	0,0454	0,0482	0,0764
Standard deviation	0,001746107			0,001574802			0,003987759			0,014000317		
Average	0,073133333			0,0748			0,063866667			0,056666667		
0,4 M	0,1116	0,1116	0,1178	0,1018	0,1058	0,0992	0,0808	0,0892	0,09	0,0838	0,0692	0,0756
Standard deviation	0,002922708			0,00271457			0,004161196			0,005975506		
Average	0,113666667			0,102266667			0,086666667			0,0762		
0,7 M	0,1608	0,1564	0,1518	0,1362	0,1122	0,1188	0,1	0,0958	0,0954	0,0898	0,094	0,0964
Standard deviation	0,003674537			0,010123241			0,002080598			0,002727636		
Average	0,156333333			0,1224			0,097066667			0,0934		
1 M	0,165	0,1712	0,169	0,1524	0,1616	0,1542	0,1006	0,1182	0,103	0,1092	0,1026	0,1018
Standard deviation	0,00256645			0,003981066			0,007792874			0,003315955		
Average	0,1684			0,156066667			0,107266667			0,104533333		

d) Fricke dosimetry tests

Table 12: Ferric ion production using air and argon (μmol)

	Temperature											
Gas	10 °C			20 °C			30 °C			40 °C		
Air	0,3641329	0,430132	0,3208921	0,37096	0,3959954	0,3072371	0,3482009	0,4073736	0,2913063	0,2867546	0,2480654	0,2253072
Standard deviation	0,044918438			0,037364923			0,047387339			0,025365276		
Average	0,371719011			0,358064027			0,348960704			0,253375816		
Argon	0,3299954	0,2890305	0,3390987	0,3072371	0,3231679	0,4483384	0,4710969	0,3117888	0,3800637	0,2116525	-	-
Standard deviation	0,02177621			0,063097038			0,065258119			0		
Average	0,319374905			0,359581247			0,387649826			0,2116525		